香港中文大學
The Chinese University of Hong Kong

The Chinese University of Hong Kong

Earth System Science Programme

Tropical Cyclone Intensity Forecast using ECMWF EPS with Machine Learning

Author:

Chan Ming Hei Kenneth[a]

[a]Department of Physics,
The Chinese University of Hong Kong

Supervisor:

Prof. Tam Chi Yung Francis[a]

Mr. Wong Wai Kin[b]

[a]Earth System Science Programme,
The Chinese University of Hong Kong
[b]Hong Kong Observatory

ESSC4820 Senior Project II

May 19, 2020

Abstract

Numerical weather prediction models provide tropical cyclone (TC) intensity and track forecasts for up to ten days. Ensemble prediction systems (EPS) were introduced to model alternative scenarios and produce probabilistic forecasts. The European Centre for Medium-Range Weather Forecasts (ECMWF) model was one of the best-performing models in TC forecasts. However, systematic negative biases were observed in its performance. A machine learning model based on XGBoost, a decision-tree-based machine learning algorithm, is presented here, in which various predictors such as selected percentiles of ensemble members in maximum wind and minimum pressure of previous TC cases were regressed to forecast a deterministic maximum wind of a TC. This XGBoost model was found to reduce the negative biases of ECMWF EPS and also enhance the overall performance. It is hoped that this machine learning model will introduce a new avenue for TC forecasts for the pursuit of higher accuracy.

Contents

List of Figures

List of Tables

1 Introduction

Destructive winds, torrential rain and storm surges from tropical cyclones (TC) bring extensive damage to coastal areas and have cost hundreds of thousands of people's lives in the past few decades (Doocy, Dick, Daniels, & Kirsch, 2013). Numerical weather prediction (NWP) assimilates atmospheric data and propagates via a series of mathematical differential equations and physical laws that describe the dynamics of the atmosphere. NWP simulates the evolution of the atmosphere for local meteorological agencies to assess the weather condition and evolution. If the models were accurate, agencies could issue timely warnings to the general public and could effectively mitigate damages brought by weather hazards (Bonavita et al., 2017).

However, NWP model accuracy is limited due to the chaotic nature of the atmosphere and the initialization error. The chaotic nature of the atmosphere originates from the nonlinearity of atmospheric processes so that slight differences in the initial conditions generate errors that amplify over time and may ultimately develop into totally different regimes, hence limiting its predictability especially in longer forecast periods. The initialization error attributes to various factors, including the sparse observations, especially over oceans. For TC forecasts, NWP centres bogus a tropical cyclone vortex into the analysis stage (P. Y. Chen & Chan, 2010), which may not represent the "real" cyclone in the atmosphere well. The finite grid representation of atmosphere and approximations made in equations applied in NWP models, which intend to achieve realistic general flow and reasonable computational time, also lead to a loss of information in the continuous atmosphere. For instance, the intense small-scale features in a TC such as its steep pressure gradient near its centre, is not acknowledged and will be rejected by the model analysis. This results in the smoothing out of the vortex which appears too large and weak in the model (Ander-

sson & Hollingsworth, 1988). Furthermore, Bonavita et al. (2017) pointed out that even if there were observations, such as dropsondes being made, the assimilated data may not be representative due to various measurement errors. Parametrization and approximation for sub-grid and not well understood physical processes introduce yet another source of error.

To cater to the chaotic nature of atmosphere and the intrinsic measurement uncertainty and error, ensemble approaches were developed to model alternative scenarios. The initial conditions were slightly perturbed and allowed to propagate again. The perturbed run will likely give a different result as the unperturbed "control" member. A number of perturbed members with different perturbations and the control member form the ensemble forecast and is further interpreted by meteorologists to assess the probability of the occurrence of certain weather events (e.g. the passage of a tropical cyclone and rainfall rate exceeding a certain threshold) or the probable range or spread of measurable parameters (e.g. wind speed, pressure and precipitation).

Yet, ensemble forecast generates multiple scenarios at the cost of reduced grid resolution. It is reasonable to infer that the TC vortices are also weaker than in reality. P. Y. Chen and Chan (2010) found that the Japan Meteorological Agency (JMA) ensemble prediction system (EPS) under-predicted TC's intensity and extent of changes, especially for stronger cyclones. In this study, we focused on the EPS output of the European Centre for Medium-Range Weather Forecasts (ECMWF) model and it was discovered that ECMWF EPS also underestimated the intensity of TCs yet the model was generally skillful in forecasting the trend of intensity change. This discovery prompted the search for a method to forecast TC intensity and detect potential rapid intensification or weakening based on the skills of the EPS model.

There has been previous research on the usage of various means of machine learning, covering the forecasts or estimations of number of TCs in a TC season (Richman, Leslie, Ramsay, & Klotzbach, 2017), TC tracks (Giffard-Roisin et al., 2020), TC wind field (Loridan, Crompton, & Dubossarsky, 2017) and TC intensity (P. Y. Chen & Chan, 2010). It has been shown that the forecast error could be reduced upon the application of machine learning. In this study, we choose the XGBoost (Extreme Gradient Boosting) library,

which is based on the gradient boosting algorithm, to generate a deterministic forecast of TC intensity for five days or more. The predictors solely come from the EPS output of the ECMWF model and we hope this framework could generate a forecast promptly when the EPS products arrive at operational centres such that it could be referenced by forecasters for real-time assessment of TC development.

As machine learning, in particular the gradient boosting algorithm, is rather new in this field, the algorithm and relevant applications will be reviewed in the next chapter. The source of errors of NWP models and techniques in forecasting rapid intensity changes of TCs will also be discussed. The data set used in this study follows in Section 3. The methodology is presented in Section 4. The study results are presented in Section 5 and discussed in Section 6. Finally, conclusions and suggestions for further exploration of machine learning in meteorology are made in Section 7.

2 Literature Review

2.1 XGBoost and its application

Established in 2014, XGBoost has become a popular machine learning method in data science. The method was based on the gradient boosting algorithm which is composed of weak learners made of decision trees. We define a loss function $l(\hat{y}_i, y_i)$ that measures the difference between the prediction $\hat{y}_i$ and the true value y_i. The two most common practices of the loss function are the absolute-error loss:

$$l(\hat{y}_i, y_i) = \sum_i |\hat{y}_i - y_i| \tag{1}$$

and the squared-error loss:

$$l(\hat{y}_i, y_i) = \sum_i \frac{1}{2}(\hat{y}_i - y_i)^2 \tag{2}$$

One may choose the base-learner function that updates the model to be maximally correlated to the negative gradient of the loss function (Natekin & Knoll, 2013). Note that for the classic squared-error loss, the gradient of the loss is just the residual $(\hat{y}_i - y_i)$ and the newly-built weak learners would gradually fit the errors. In the XGBoost method, an extra

regularization parameter was added to avoid over-fitting by penalizing complex trees (T. Chen and Guestrin, 2016). A randomization parameter was also introduced to reduce the correlation between trees.

In light of the pursuit of a simple and general model, XGBoost supports the identification of feature importance. In general, the "gain" option is indicative of the average reduction of the loss function when the feature is used in splits. In modeling variables that are believed to be influenced by many features, it is important to identify significant features to retain in the model and to remove features that contribute little to the model. This reduces the complexity of the model and could avoid over-fitting.

In a study on the prediction of $PM_{2.5}$ concentration in Tehran by Zamani Joharestani, Cao, Ni, Bashir, and Talebiesfandarani (2019), there were around twenty features assimilated into the model while they demonstrated differential importance to the model performance. The authors removed features sequentially according to mean absolute error (MAE) metrics but the model performance did not decrease when less important features were removed from the model. We also observe that the importance rankings according to the XGBoost built-in feature importance and the MAE metrics generally agreed for most features. We question if the built-in importance is indicative of the variation in model performance by the MAE or root-mean-square error (RMSE) metrics.

2.2 Sources of errors of NWP models

The fundamental ideas of numerical weather prediction (NWP) were first developed by Lewis Fry Richardson, where some basic equations that govern the dynamics of the atmosphere were identified and atmospheric variables at given latitude, longitude and height in an instant were provided to describe the state of the atmosphere. The time-derivatives were then transformed to finite time differences Δt, and the state of the atmosphere after Δt, $2\Delta t$, $3\Delta t$ and so on could be yielded (Lynch, 2008).

However, Richardson's first attempt to arithmetically calculate the atmosphere gave a calamitous and unrealistic pressure change of 145 hPa over 6 hours. It was not until the introduction of digital computers and the expansion of meteorological observation network that the concept of NWP flourished.

Although supercomputers are used in modern NWP models, certain complexity of the atmosphere has to be simplified and grid resolution is limited to generate the prediction at a faster pace than the atmosphere, for the model to be useful. Some unresolved, sub-grid or not well understood physical processes are parametrized or approximated and become a source of error. Moreover, despite the expansion of meteorological observation network and the introduction of radiosondes, many regions, especially the oceans, are void of data. These data-void regions have their atmospheric variables estimated by making use of neighbouring data points, in order to simulate a continuous atmosphere. Such estimation may be erroneous and is known as the initialization error. Another source of initialization error is that local observations may be easily affected by local or sub-grid scale flows and become unrepresentative of large-scale general flows. In such cases, the observations are modified to maintain a dynamically consistent initial state to properly start the propagation (Lynch, 2008).

It should be noted that some authenticity in the state of the atmosphere is lost during the modification, or in technical terms, the data assimilation stage. This impacts the analysis of tropical cyclones that often results in a weaker-than-actual vortex. The maximum wind of a TC occurs near its centre where the steepest pressure gradient is found. The Rossby number (Ro) was defined as:

$$Ro = \frac{V}{rf} \tag{3}$$

where V is the characteristic axial wind velocity, r is the radius from the centre and $f = 2\Omega \sin\phi$ is the Coriolis parameter, with Ω = 7.292 $\times$ 10^{-5} s^{-1} as the angular velocity of Earth's rotation and ϕ as the latitude. At the vicinity of the eye wall, Ro is often high and could reach 100 especially for intense storms, resulting in a cyclostrophic flow near the core of the TC (Marks, 2015). The observations in cyclostrophic flow may be considered as in conflict with the outer environment of the storm, where the flow is in general gradient or geostrophic. Hence, the intense small-scale features near the core are not acknowledged and the observation data on typhoon cores will be rejected (Andersson & Hollingsworth, 1988).

Typhoon bogussing schemes were developed to simulate a more realistic vortex. Several physical parameters such as the latitude, longitude, storm size and minimum pres-

sure were specified to generate a bogus vortex. Such vortex was inserted into the large scale flow for initial analysis with the constraints that the bogus must not be in conflict with any real observations nearby and should not adversely affect the large scale flow (Andersson & Hollingsworth, 1988). Research showed that the motion of cyclones were mainly governed by the large-scale flow away from the centre (Fiorino & Elsberry, 1986, as cited in Andersson & Hollingsworth, 1988; DeMaria, 1986, as cited in Andersson & Hollingsworth, 1988). In respect of the large scale flow and a realistic forecast, the analysis often turned out to have the cyclone vortex smoothened when comparing to the bogus.

NWP forecasting skills have improved over the years and finer resolutions have been achieved. There are also more satellite and data observations available for a better simulation of the atmosphere. Bogussing schemes were also optimized to achieve a dynamically and physically consistent environment. However, as to maintain a realistic general flow, the intense features were still unresolvable and caused the underestimation in TC intensity.

Bogussing schemes usually adopt the Rankine vortex or the gradient wind balance. In the Rankine vortex, the tangential velocity v at a radius r from the centre is given by:

$$v = A(z)F(r) \tag{4}$$

$$F(r) = \frac{v_m}{r_m} r, r \leq r_m \tag{5}$$

$$F(r) = \frac{v_m}{r_m^\alpha} r^\alpha, r \geq r_m \tag{6}$$

where v_m is the maximum wind of the bogus which is assumed to be lower than the reported value. r_m is the radius of maximum wind and $A(z)$ reflects the amplitude and height dependence. α is a parameter typically around -0.5.

For the gradient wind relationship, v is given by:

$$v(r) = \sqrt{\frac{r}{\rho}\frac{\partial P}{\partial r} + \frac{f^2 r^2}{4}} - \frac{r|f|}{2} \tag{7}$$

where P is the bogus pressure as a function of r and ρ is the density of air, assumed constant at 1.2 kg m^{-3} (D. Wang, Liang, Ying, & Wang, 2008).

We note that these relationships do not represent a cyclostrophic flow well, which is given by:

$$v(r) = \sqrt{\frac{r}{\rho}\frac{\partial P}{\partial r}} \tag{8}$$

Such flow may occur near the centre of intense cyclones where the Coriolis force is negligible when compared with the centrifugal and pressure gradient forces. Ultimately, even though the modeling and bogussing techniques have been improved, it is still very often that NWP fails to give an accurate representation of TCs, especially for severe typhoons.

2.3 Ensemble prediction systems

To counter the forecast errors due to the initialization errors, ensemble prediction systems (EPS) were developed to simulate alternative scenarios of the atmosphere. Each ensemble member was initialized with a slightly perturbed state e_j:

$$e_j(t=0) = e_0(t=0) + \delta e_j(t=0) \tag{9}$$

where e_0 was the operational analysis at $t = 0$ and δe_j was the initial perturbations, with its amplitude scaled to be comparable to the initial error estimates. The propagation of e_j was then given by:

$$\frac{\partial e_j}{\partial t} = A(e_j, t) + P_j^{'}(e_j, t) \tag{10}$$

where A and $P^{'}$ represented the non-parametrized and parametrized physical processes respectively. $P^{'}$ was obtained through perturbing the unperturbed diabatic tendency P:

$$P_j^{'}(e_j, t) = [1 + \langle r_j(\lambda, \phi, \sigma \rangle_{D,T}]P(e_j, t) \tag{11}$$

where r_j was a random number with intervals [-0.5, 0.5], depending on the grid point's latitude λ, longitude ϕ and vertical hybrid coordinate σ. The same r_j was used within a $D \times D$ degree box and over T time steps. The final adoption for the ECMWF EPS was D = 10 and T = 6 hours (Buizza, 2002).

There have been studies reviewing the performance of EPS in TC intensity forecasts. P. Y. Chen and Chan (2010) reviewed the Japan Meteorological Agency's (JMA) EPS in the prediction of TC intensity. Although the ensemble mean intensity was considered to perform better than the control or individual member forecasts as it filtered out uncertain components in the forecast, it tended to smooth the change in intensity. In general it demonstrated skills in forecasting intensity changes but was unable to capture the processes of rapid intensification or weakening. Strong typhoons were hence rarely forecast

and would be detrimental to hazard prevention. It was also found that the EPS had positive biases in the TC initial central pressure, i.e. it analyzed a vortex which was too shallow. The initial maximum wind also demonstrated systematic biases against the best track estimates for different storm strengths. Recalling the initialization errors and drawbacks of initialization and bogussing schemes, post-processing methods should be sought to generate better forecasts while retaining the skills of the EPS.

2.4 Tropical cyclone rapid intensity change

Rapid intensity change in TCs has been a tricky problem for meteorologists, especially for rapid intensification (RI) as it may bring huge unexpected damage to lives and properties. There have been various definitions for RI, in which the rate of 30 kt/24 h was adopted by Kaplan and DeMaria (2003), Edson and Ventham (2008) (as cited in Mei & Jiang, 2012) and B. Wang and Zhou (2008). Holliday and Thompson (1979) defined RI as the decrease in central pressure by 42 hPa/day. Ventham and Wang (2007) defined different thresholds for RI with respect to the storm intensity, where an increase in maximum wind by 35 knots and 40 knots over 24 hours defined an RI event for weak and strong storms respectively on the condition that the TC did not weaken during the past six hours before the RI event.

It was found that the occurrence of RI in a TC may hint at a high peak intensity. Almost all TCs which underwent RI ultimately reached typhoon strength or above while most of them intensified to a super typhoon. Most strong typhoons experienced RI at least once in their life cycles (Mei & Jiang, 2012). This reflects the cruciality for meteorologists to understand the principles behind RI as early warnings and prompt precautions could be made to effectively mitigate the weather hazard which leads to casualties and loss of properties.

Statistical approaches have been taken to identify the variables conducive for RI to occur. Mei and Jiang (2012) identified that 12-hour intensity change, sea surface temperature (SST), vertical wind shear (VWS) and other meso-scale atmospheric variables may influence the occurrence of RI. However, it is noted that satisfying the threshold for one variable is not indicative of RI as complex physical processes lie behind RI and it requires a simultaneous satisfaction of multiple atmospheric variables' thresholds. Although

favourable conditions for RI to occur have been qualitatively explained (Hu, Duan, Yu, Yu, & Du, 2005), conditions where RI is certain to happen have not been found. However, Mei and Jiang (2012) identified a region over the seas east of the Philippines where RI was more likely to take place. One may hypothesize if favourable atmospheric conditions are more likely to occur in these preferred regions such that RI events are more likely to happen.

Shaiba and Hahsler (2016) combined statistical approaches with machine learning methods to predict the occurrence of RI. It was shown that various machine learning models were skillful in detecting RI. Coupling statistical models in forecasting RI with intensity forecast models was also found to improve intensity forecast by taking the probability of RI into account (Kaplan et al., 2015; Shaiba & Hahsler, 2016).

3 Data set

The ECMWF EPS TC data was studied in this project. The data covers TC over the western North Pacific (north of the Equator, 100°to 180°E) from January 1, 2015 to August 3, 2019. The data includes forecasts of the TC intensity (minimum pressure and maximum wind at the centre) of the 51 ensemble members, the ensemble mean latitude and longitude, the base time and the forecast lead time. There were two EPS runs every day at 00 and 12 UTC respectively. The forecast data are in 6-hour intervals, reaching a maximum range of 240 hours. A total of 121 TC cases with 24953 base time-lead time pairs are included.

Among the 121 cases, a quarter was randomly chosen as the verification set and the rest remained as the training set for the proposed model. The two groups of TC were tabulated in Tables 1 and 2 below respectively.

In evaluating the EPS and our proposed model performances, Hong Kong Observatory's (HKO) best track (BT) intensity was adopted as the ground truth.

The below plot shows that the EPS mean has been generally underestimating the maximum wind of TCs.

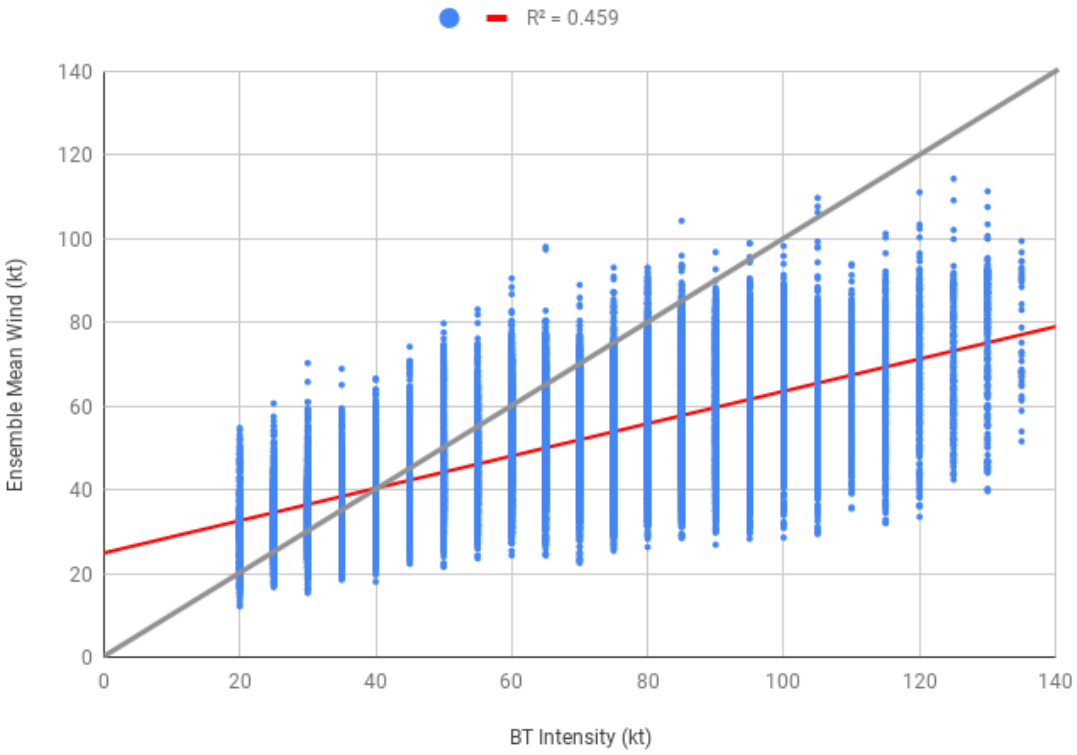

Figure 1: ECMWF EPS Mean vs HKO BT Intensity (All TC cases)

The number of forecast samples for different lead hour ranges and best track maximum wind distribution are shown in Figures 2 and 3 below.

Training Set								
TCID	Intensity	TC Name	TCID	Intensity	TC Name	TCID	Intensity	TC Name
1502	Super T	Higos	1607	TS	Chanthu	1723	T	Damrey
1503	TS	Bavi	1610	ST	Lionrock	1724	TS	Haikui
1504	Super T	Maysak	1615	TD	Rai	1802	TS	Sanba
1505	TS	Haishen	1616	ST	Malakas	1803	Super T	Jelawat
1506	Super T	Noul	1617	ST	Megi	1804	TS	Ewiniar
1507	Super T	Dolphin	1618	Super T	Chaba	1805	STS	Maliksi
1509	Super T	Chan-hom	1619	TS	Aere	1806	TS	Gaemi
1510	T	Linfa	1620	Super T	Songda	1807	T	Prapiroon
1511	Super T	Nangka	1622	Super T	Haima	1810	STS	Ampil
1512	T	Halola	1623	T	Meari	1811	STS	Wukong
1513	Super T	Soudelor	1624	TS	Ma-on	1812	T	Jongdari
1514	TS	Molave	-	TD	TD1212	1813	T	Shanshan
1515	Super T	Goni	1626	Super T	Nock-ten	1814	TS	Yagi
1516	Super T	Atsani	-	TD	TD0108	1816	STS	Bebinca
1517	ST	Kilo	-	TD	TD0414	1817	TS	Hector
1518	STS	Etau	1702	STS	Merbok	1818	TS	Rumbia
1519	TD	Vamco	1703	STS	Nanmadol	1819	ST	Soulik
1521	Super T	Dujuan	1705	Super T	Noru	1820	ST	Cimaron
1522	ST	Mujigae	1707	TS	Roke	1821	Super T	Jebi
1523	STS	Choi-wan	1711	TS	Nalgae	1822	Super T	Mangkhut
1524	Super T	Koppu	1712	ST	Banyan	1824	Super T	Trami
1525	Super T	Champi	1713	Super T	Hato	1825	Super T	Kong-rey
1526	Super T	In-fa	1716	STS	Mawar	1827	TD	Toraji
1527	ST	Melor	1717	TD	Guchol	1828	T	Man-yi
1601	Super T	Nepartak	1718	Super T	Talim	1829	STS	Usagi
1602	TS	Lupit	1719	ST	Doksuri	-	TD	TD1225
1603	STS	Mirinae	-	TD	TD1009	1902	Super T	Wutip
1604	T	Nida	1720	ST	Khanun	1903	TD	Sepat
1605	STS	Omais	1721	Super T	Lan	1904	TS	Mun
1606	TS	Conson	1722	T	Saola	1907	TS	Wipha

Table 1: Tropical Cyclones in Training Set

Verification Set								
TCID	Intensity	TC Name	TCID	Intensity	TC Name	TCID	Intensity	TC Name
1501	T	Mekkhala	1701	TD	Muifa	1727	T	Tembin
1508	TS	Kujira	1704	STS	Talas	1801	TS	Bolaven
1520	ST	Krovanh	1706	TS	Kulap	1808	Super T	Maria
1608	TS	Dianmu	1708	TS	Sonca	1809	TS	Son-Tinh
1609	STS	Mindulle	1709	T	Nesat	-	TD	TD0721
1611	TS	Kompasu	1710	TS	Haitang	1815	STS	Leepi
1612	ST	Namtheun	1714	STS	Pakhar	-	TD	TD0823
1613	TD	Malou	1715	T	Sanvu	1823	TS	Barijat
1614	Super T	Meranti	-	TD	TD0923	1826	Super T	Yutu
1621	Super T	Sarika	1725	TS	Kirogi			
1625	STS	Tokage	1726	TS	Kai-tak			

Table 2: Tropical Cyclones in Verification Set

Classification	Maximum 10-minute mean wind near the centre	
	km/h	knots
Tropical Depression (TD)	41-62	22-33
Tropical Storm (TS)	63-87	34-47
Severe Tropical Storm (STS)	88-117	48-63
Typhoon (T)	118-149	64-80
Severe Typhoon (ST)	150-184	81-99
Super Typhoon (Super T)	$\geq$185	$\geq$100

Table 3: HKO Classification of Tropical Cyclones

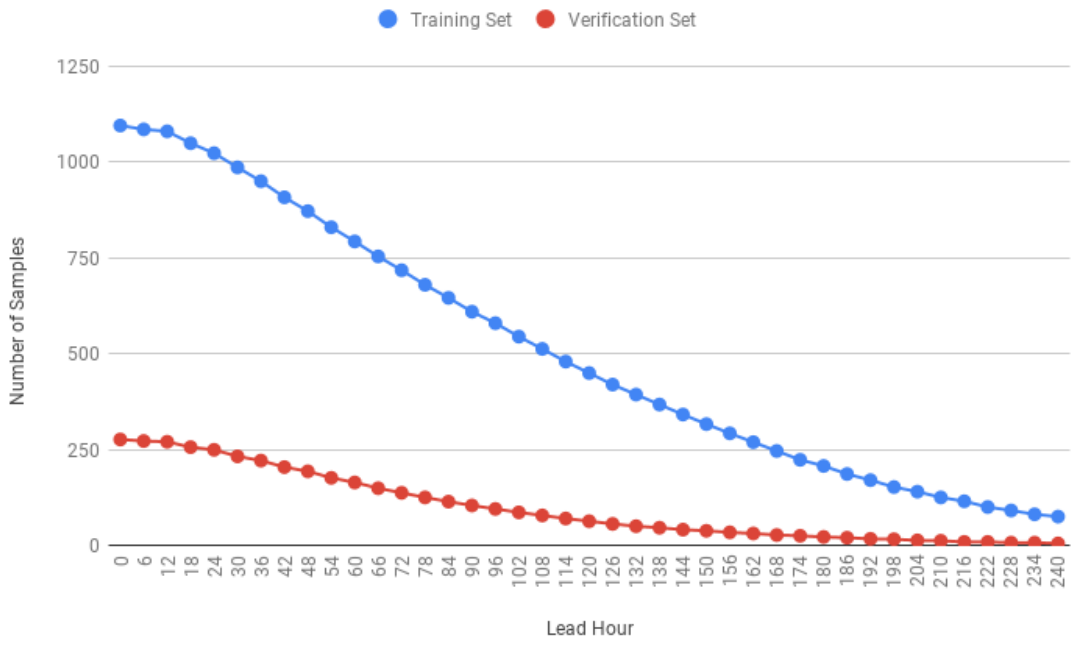

Figure 2: Number of samples in the ECMWF EPS TC dataset in January 1, 2015 to August 3, 2019

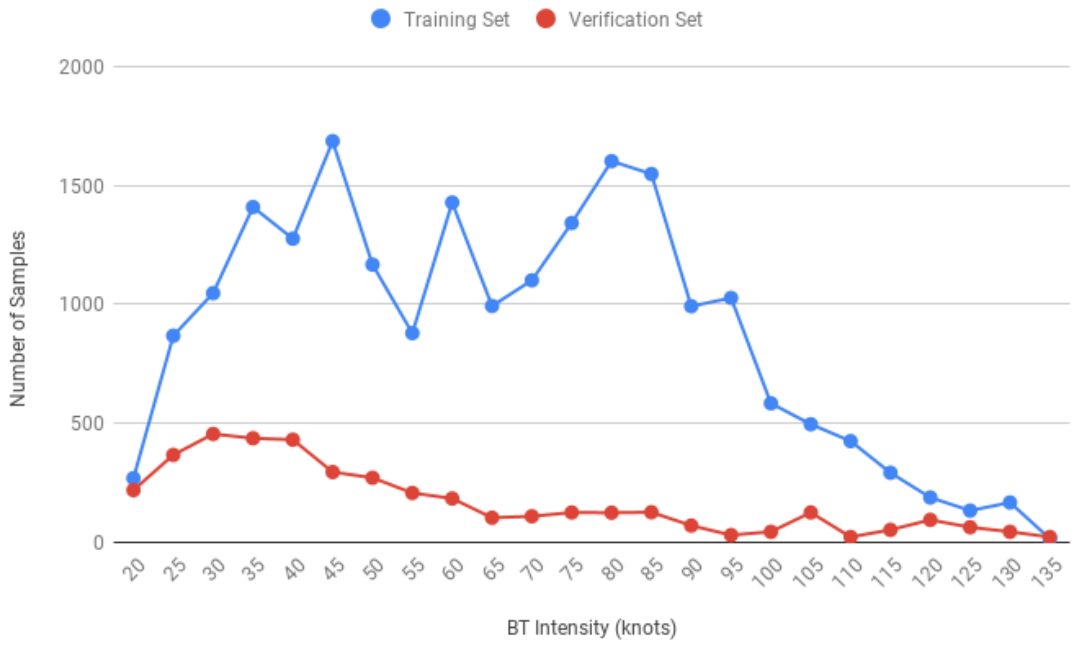

Figure 3: BT intensity distribution of the ECMWF EPS TC dataset in January 1, 2015 to August 3, 2019

4 Methodology

The 5th, 25th, 50th, 75th and 95th percentiles of the 51 ensemble members, in terms of pressure and maximum wind, were calculated respectively and were adopted to be among the predictors of the maximum wind of the TC.

A total of 15 features derived from ECWMF EPS forecast were chosen to be predictors of the maximum wind of TC (see Table 4 below).

Abbreviation	Predictor
ENS_MEAN_LAT	Ensemble Mean Latitude
ENS_MEAN_LON	Ensemble Mean Longitude
ENS_MEAN_PRESSURE	Ensemble Mean Central Pressure
ENS_MEAN_WIND	Ensemble Mean Maximum Wind
FCST_HR	Lead Time (Hour)
PRESSURE_0.05	5th Percentile Central Pressure
PRESSURE_0.25	25th Percentile Central Pressure
PRESSURE_0.5	50th Percentile Central Pressure
PRESSURE_0.75	75th Percentile Central Pressure
PRESSURE_0.95	95th Percentile Central Pressure
WIND_0.05	5th Percentile Maximum Wind
WIND_0.25	25th Percentile Maximum Wind
WIND_0.5	50th Percentile Maximum Wind
WIND_0.75	75th Percentile Maximum Wind
WIND_0.95	95th Percentile Maximum Wind

Table 4: Predictors Used in Formulation of XGBoost Model

In pursuit of a reduction in model complexity, we sought to identify features which were considered important by the model and to retain only the most significant features in the model. A simple trial model was first built by including all features as predictors. The Python version XGBoost Regressor model was built on a computer platform loaded with a GeForce® GTX 1080 Ti graphic card.

For simplicity, all parameters were set to default except the number of gradient boosted trees (*n_estimators*) and the maximum tree depth for base learners (*max_depth*) which we varied to optimize the model.

In the first trial we adopted the values of *n_estimators* = 100 and *max_depth* = 5 to train the model using the training set data. Next, the built-in *plot_importance* function was used to obtain features' importance based on the fitted trees. Each feature's importance was calculated based on the average gain of splits which used the feature.

After obtaining the importance of each feature, the model was used to predict the maximum wind of TCs in the verification set. The results were verified against the HKO BT intensity using the RMSE metrics:

$$RMSE = \sqrt{\sum_{i=1}^{n} \frac{(\hat{v}_i - v_i)^2}{n}} \tag{12}$$

To account for the general time dependence of the forecast accuracy, each forecast was categorized into lead time bins before calculating the RMSE value for each bin.

We trained the model again with the least important feature identified by XGBoost being removed from the set of predictors with other parameters unperturbed. The RMSE values were re-computed with the new set of forecast data. The above forecast procedure was repeated with a sequential removal of less important features according to the ranking depicted by XGBoost until only one most important feature remained as the sole predictor. We would expect the model performance to remain steady for the first few removals of features as these predictors may not contribute much to the forecast accuracy and introduce model complexity. As the set of predictors continued to shrink, we would expect the model performance to deteriorate, which would serve as a signal to keep the remaining features in the model.

As we determined the final set of predictors used in the model, we finally proceeded to vary the values of *n_estimators* and *max_depth* to determine the best pair of values for the model.

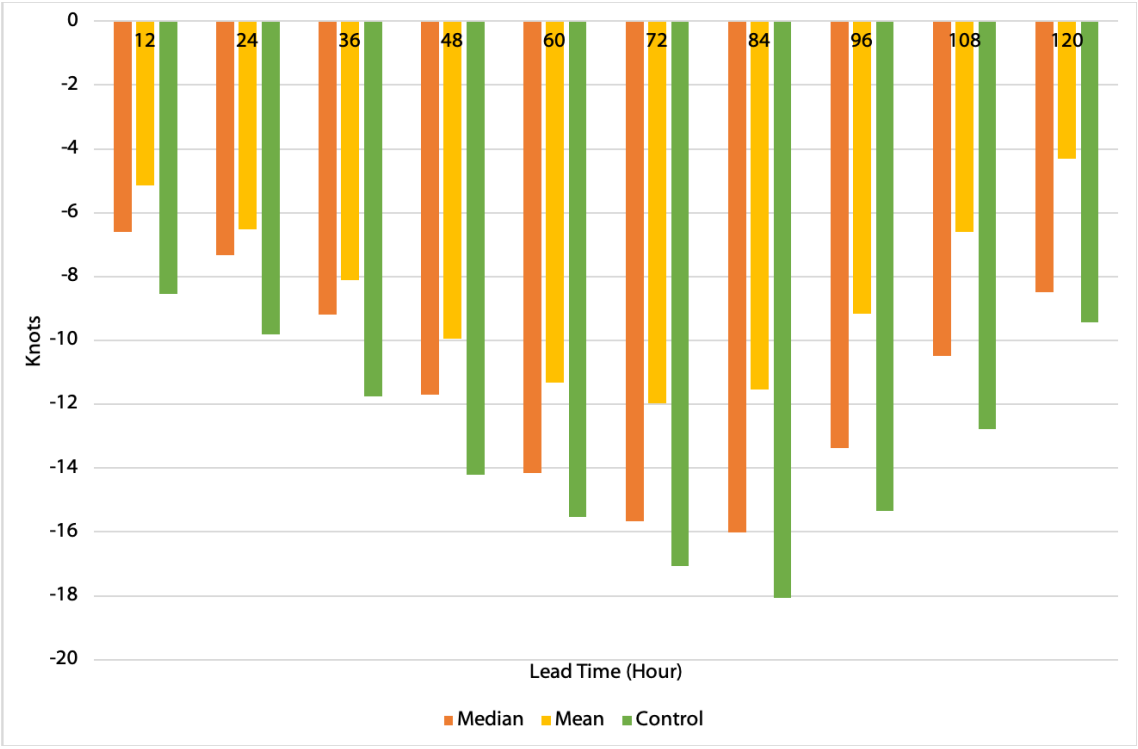

Figure 4: ECMWF EPS Forecast Mean Error (Verification Set)

5 Results

Predictors have been found to have different importances in the XGBoost model. We selected the important features to remain in the model. To generate more accurate and realistic forecasts for TCs of different strengths, we developed a consensus model with the combination of two individual XGBoost models. The consensus model was found to outperform the EPS.

5.1 ECMWF EPS

As shown in Figure 4, the EPS has underestimated the intensities of TCs. The underestimation exists over all forecast ranges and the negative bias is most significant for T+72h and T+84h forecasts.

5.2 Feature Importance

The gain method was adopted to find the feature importance. The set of predictors as listed in Table 4 demonstrated different importance in the XGBoost model. The 95^{th} and 75^{th}

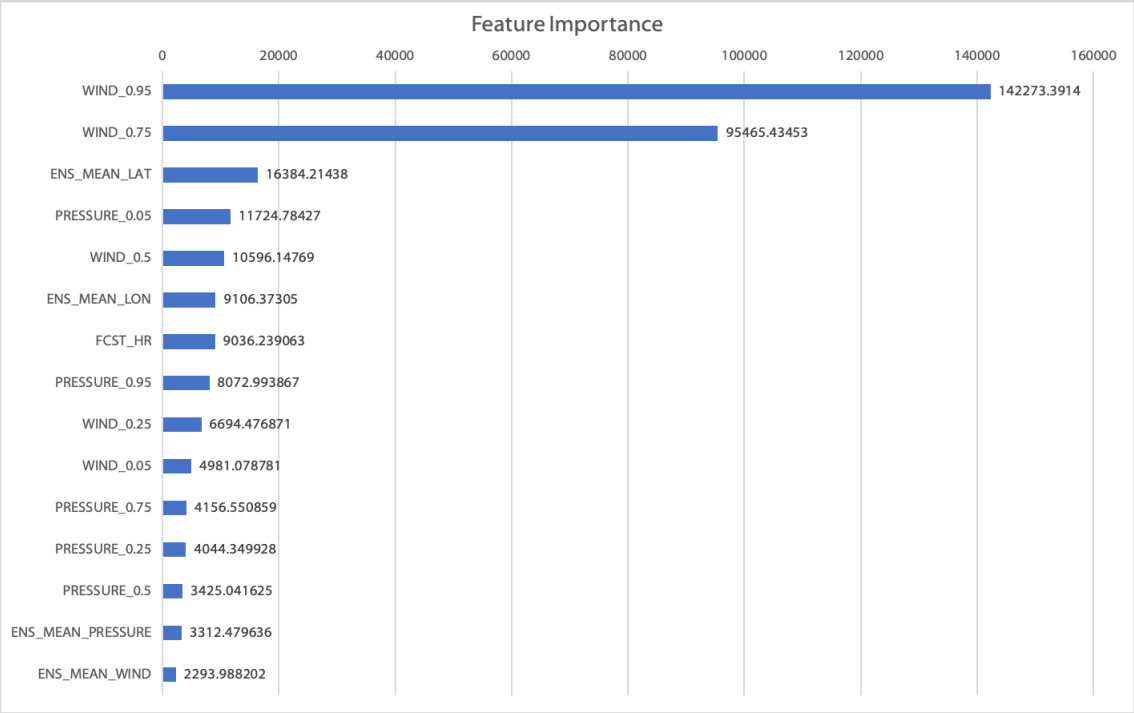

Figure 5: Feature Importance

percentiles of EPS wind members dominate the contribution, followed by the forecast location and some "stronger" EPS members. "Weaker" EPS members and ensemble means generally contribute little to the model, with ensemble mean wind and pressure being the least contributors.

Having the set of predictors sequentially removed from the model according to their ranking in the XGBoost feature importance, the forecast errors vary as a new model was trained up each time. The result is shown in Figure 6 below.

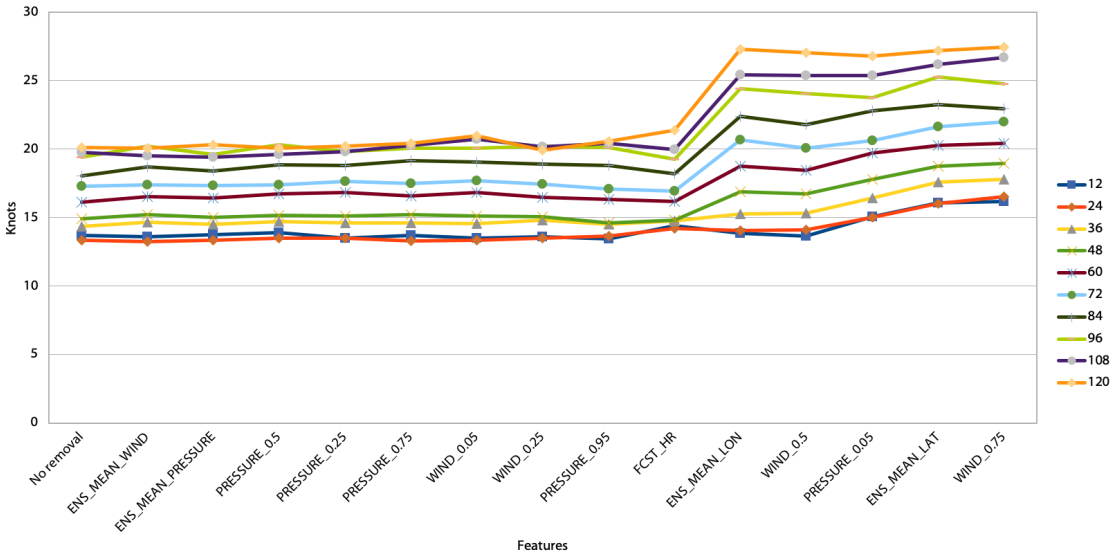

Figure 6: Forecast RMSE for Different Lead Time Hours upon Sequential Feature Removal

The leftmost column indicates the result when none of the predictors were removed. The rightmost column shows the result when WIND_0.75, the second most important feature was removed and the WIND_0.95 remained as the only predictor. We note that the forecast errors for all lead time hours remain stable when the first few less important predictors were removed. The forecast error starts to steadily increase when FCST_HR or ENS_MEAN_LON was removed for most lead time hours. Hence, we determine that the seven most important predictors are to be kept in the model, including FCST_HR and those that are more important features (Table 5).

Abbreviation	Predictor
ENS_MEAN_LAT	Ensemble Mean Latitude
ENS_MEAN_LON	Ensemble Mean Longitude
FCST_HR	Lead Time (Hour)
PRESSURE_0.05	5th Percentile Central Pressure
WIND_0.5	50th Percentile Maximum Wind
WIND_0.75	75th Percentile Maximum Wind
WIND_0.95	95th Percentile Maximum Wind

Table 5: Final Predictors Used in the XGBoost Model

5.3 Training Parameters

The values of *n_estimators* and *max_depth* were varied. In the initial trial with *n_estimators* = 100 and *max_depth* = 5, we observed that the XGBoost model often overestimated the intensities of weaker TCs (e.g. TS Dianmu in Figure 7a), while the processes of RI and peak intensities of strong TCs (e.g. Super T Maria in Figure 7b) were often successfully captured.

We propose that the forecast performance for stronger TCs and weaker TCs should be analyzed separately. We chose 63.8 knots (equivalent to the threshold of Beaufort Scale force 12, hurricane force) as the boundary. The value was chosen in light of the sample sizes in the verification set (about one third below 63.8 knots and two-thirds above 63.8 knots). The forecast performance under the variations of *n_estimators* and *max_depth* is shown in Figure 8.

As highlighted in the figure, the minimum RMSE occurs at significantly different values of *n_estimators* and *max_depth*. For the weaker TC category, the best pair is at about *n_estimators* = 15 and *max_depth* = 6. Whereas for the stronger TC category the best pair is at about *n_estimators* = 400 and *max_depth* = 4. Finer categories are not suggested as to ensure a sufficiently large sample size in each category.

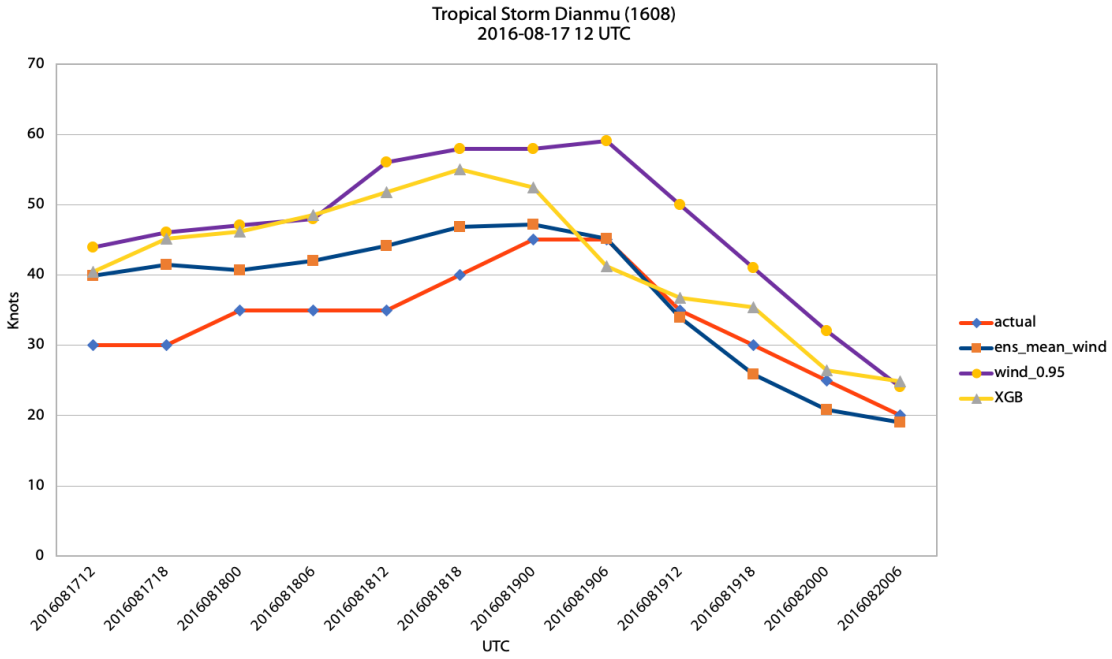

(a) Tropical Storm Dianmu (1608); Base Time 2016-08-17 12 UTC

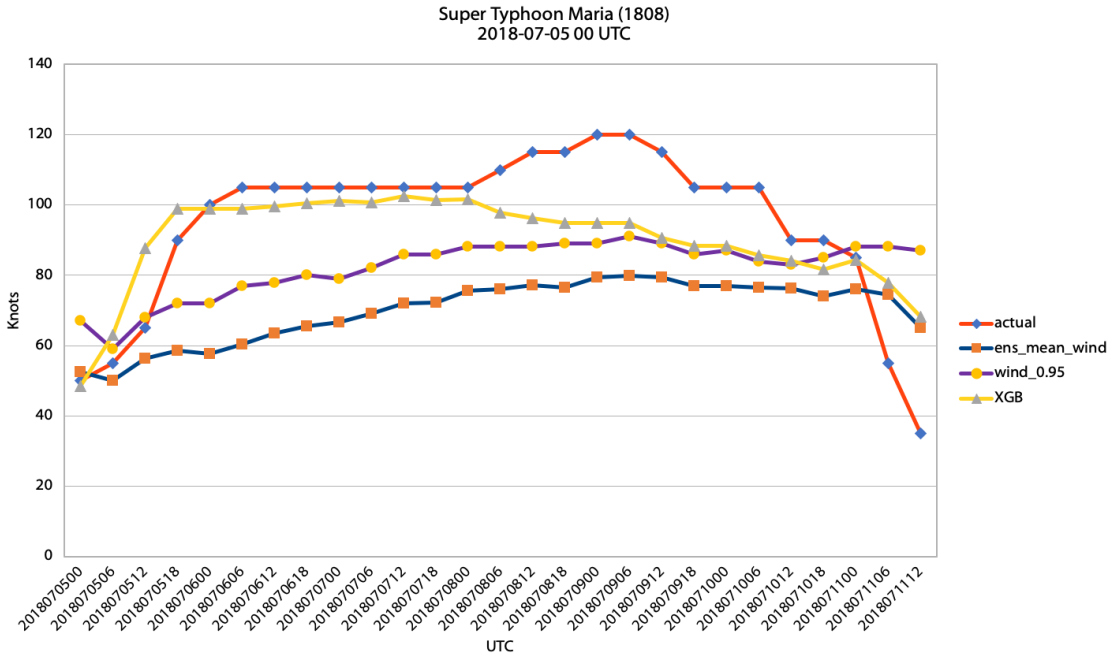

(b) Super Typhoon Maria (1808); Base Time 2018-07-05 00 UTC

Figure 7: XGBoost Model Initial Trial (*n_estimators* = 100 and *max_depth* = 5), ECMWF EPS Mean and 95th Percentile Forecast against HKO BT Intensity (Actual)

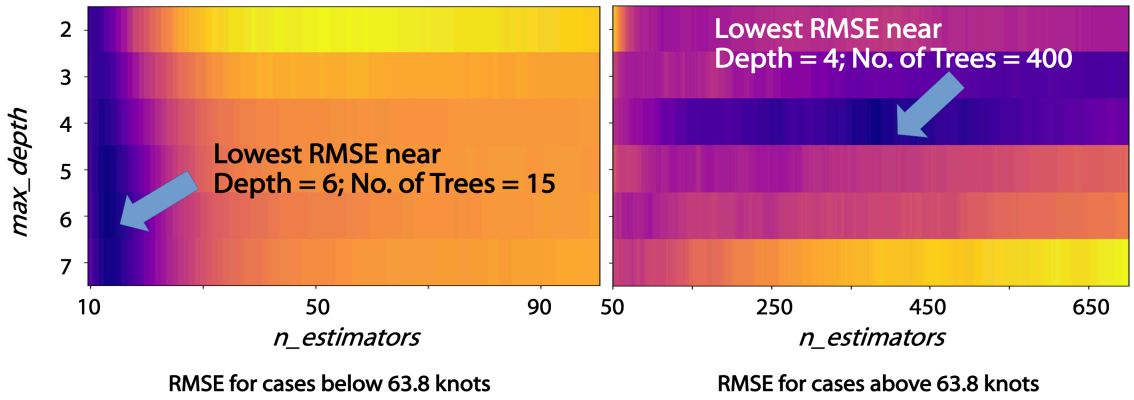

Figure 8: Forecast RMSE for Different *n_estimators* and *max_depth* Specifications

5.4 Consensus XGBoost Model

We looked for a solution which retains its ability to capture RI events and intensity peaks of stronger typhoons, while being able to produce more accurate forecasts for weaker storms. Recognizing that WIND_0.95 is the most important feature, we propose a "consensus" model, adopting WIND_0.95 as the decision node.

Two XGBoost forecast models were simultaneously and independently trained. One of them was trained with *n_estimators* = 15 and *max_depth* = 6 ("Low" model) while the other was trained with *n_estimators* = 400 and *max_depth* = 4 ("High" model). Both models take in the predictors in Table 5 and produce a maximum wind forecast value. Each forecast data is considered independently. If WIND_0.95 reports a forecast reaching 63.8 knots, the forecast value from the "High" model is adopted as the final output. Otherwise, the forecast value from the "Low" model is adopted.

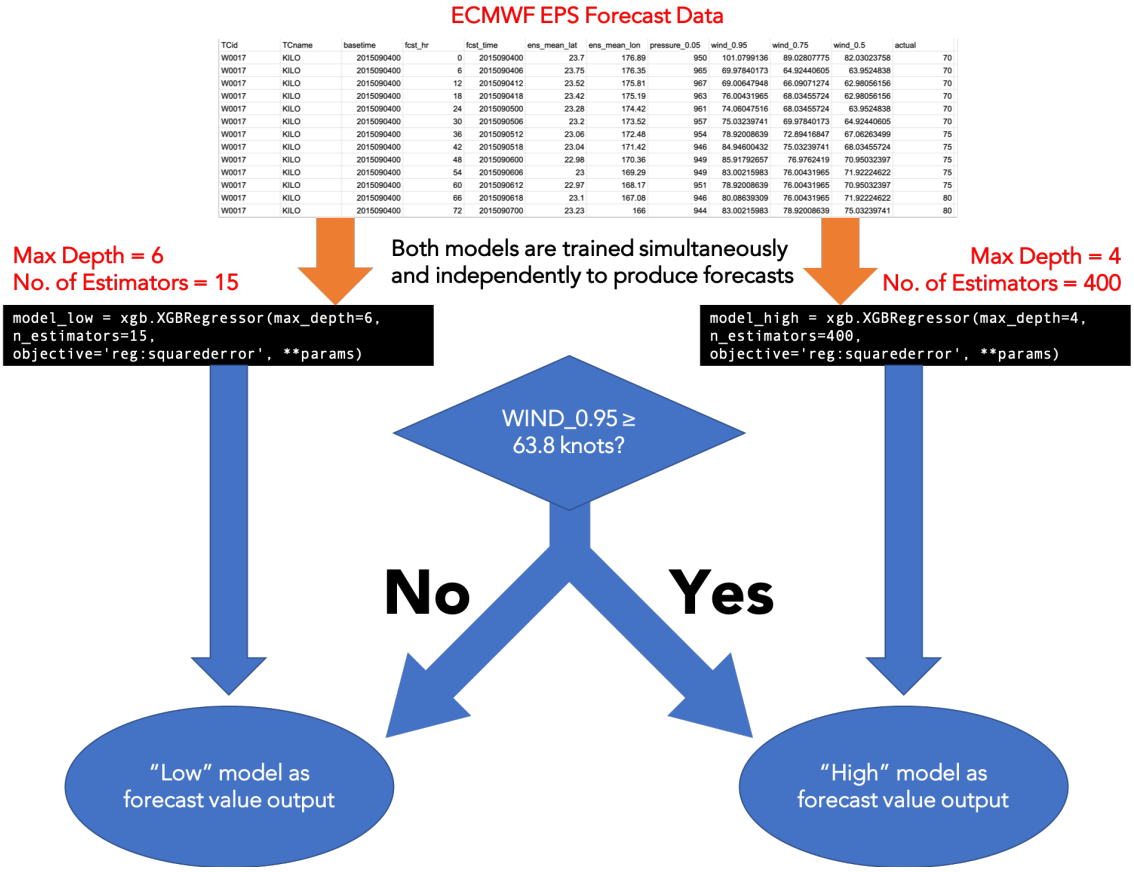

Figure 9: Schematic Diagram of the "Consensus" XGBoost Model

It should be noted that for each set of forecast of the same base time, the choice of "High" or "Low" model may vary between lead time hours depending on the value of WIND_0.95 at each lead time.

The forecast performance of the Consensus XGBoost Model and selected percentiles of ECMWF EPS is shown in Figure 10 and 11 below. It was also found that the Consensus model generally performs better than solely either the "High" or "Low" model (Figure 12).

Revisiting the forecast samples, we found that the intensity overestimation for weaker TCs is eased (e.g. TS Dianmu in Figure 13a as compared to Figure 7a) while the consensus model is still able to capture RI events and intensity peaks of severe TCs (e.g. Super T Maria in Figure 13b as compared to Figure 7b).

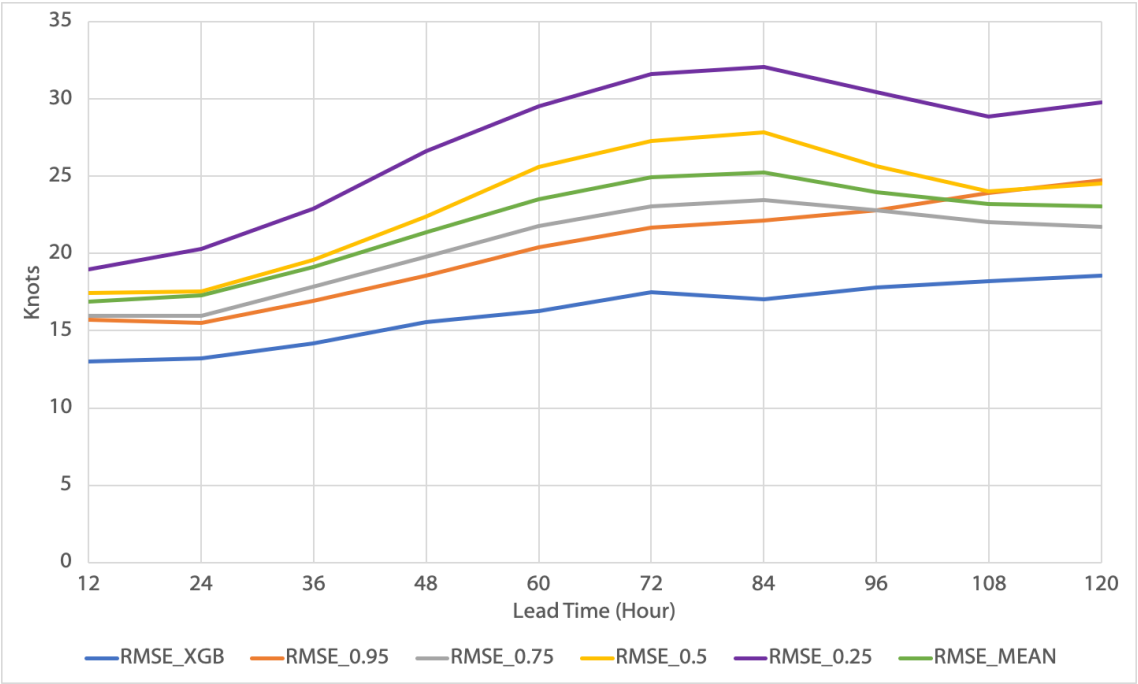

(a) Forecast RMSE

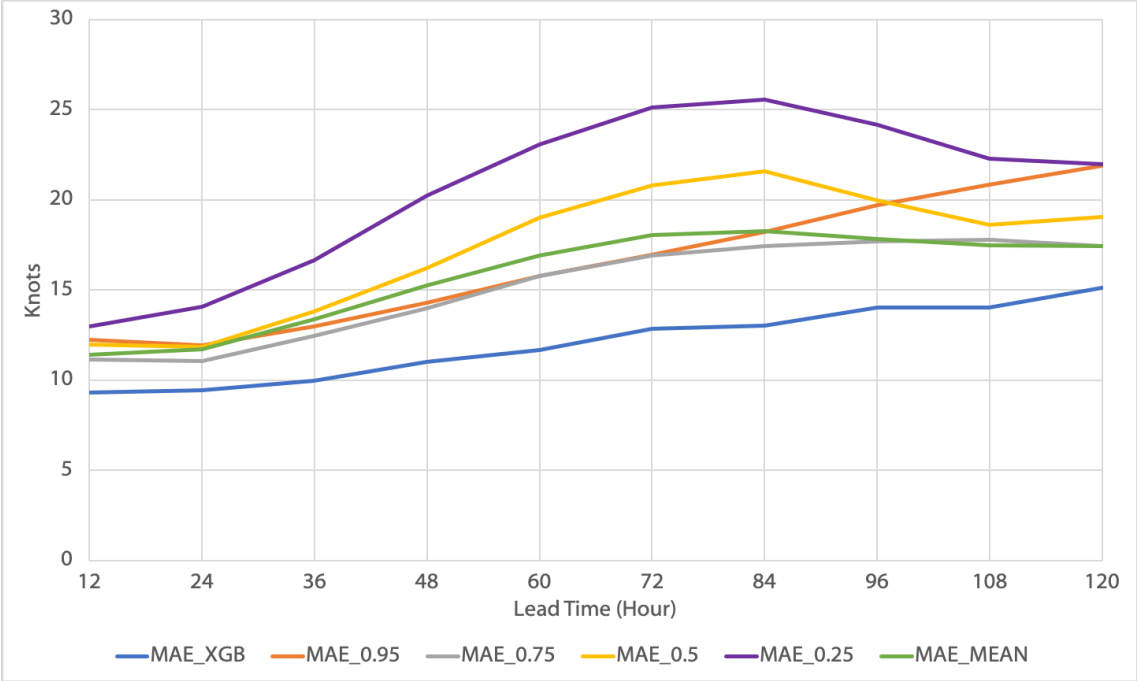

(b) Forecast MAE

Figure 10: Forecast Error of Consensus XGBoost Model (XGB), ECMWF EPS 95th (0.95), 75th (0.75), Median, 25th (0.25) and Mean Members

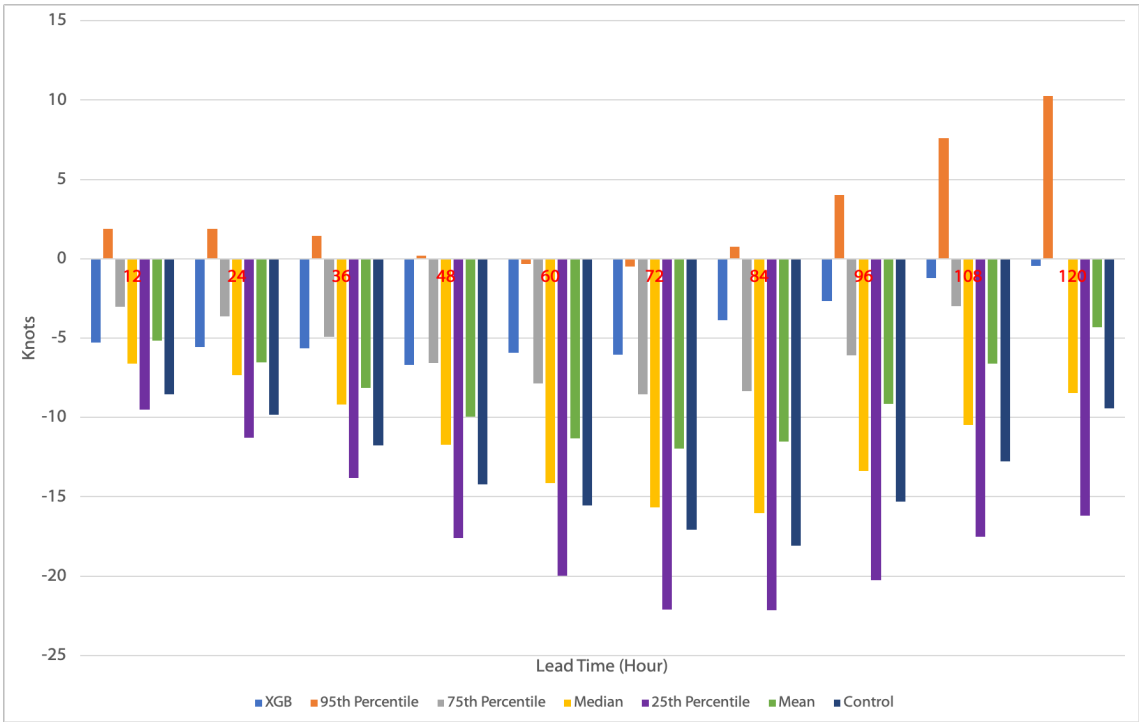

Figure 11: Forecast Mean Error of Consensus XGBoost Model (XGB), ECMWF EPS 95th, 75th, Median, 25th, Mean and Control Members

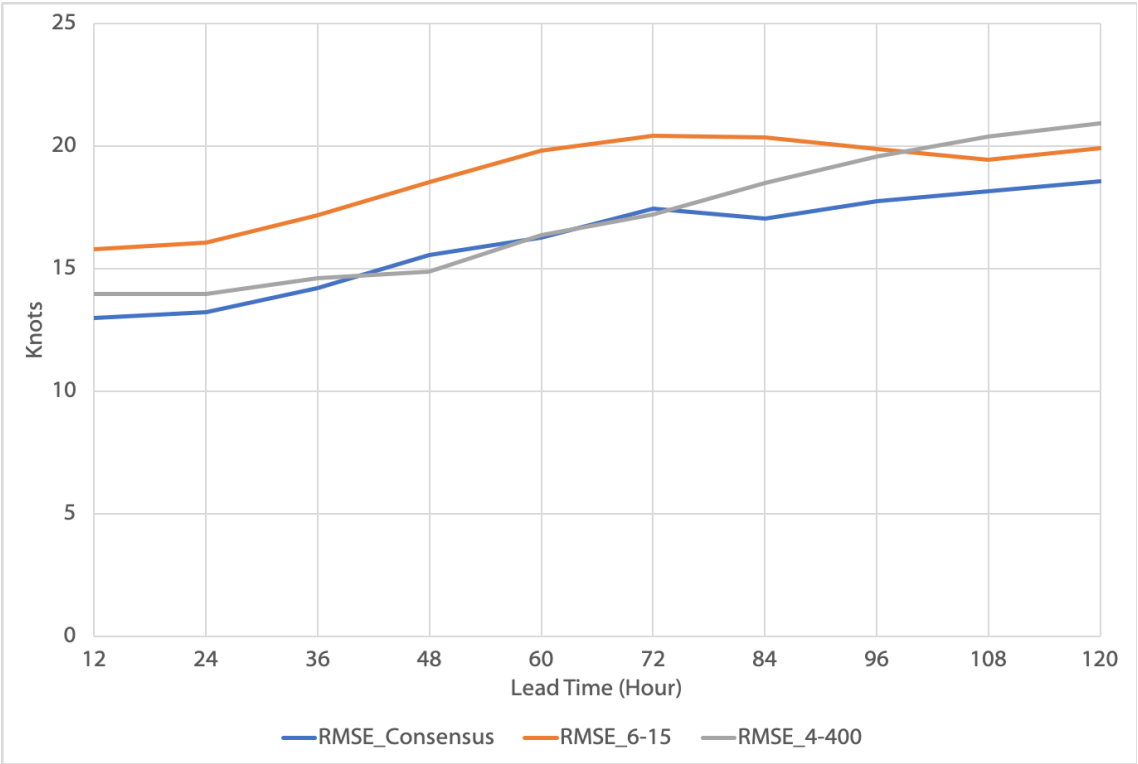

Figure 12: Forecast RMSE of Consensus, "Low" (6-15) and "High" (4-400) XGBoost Model

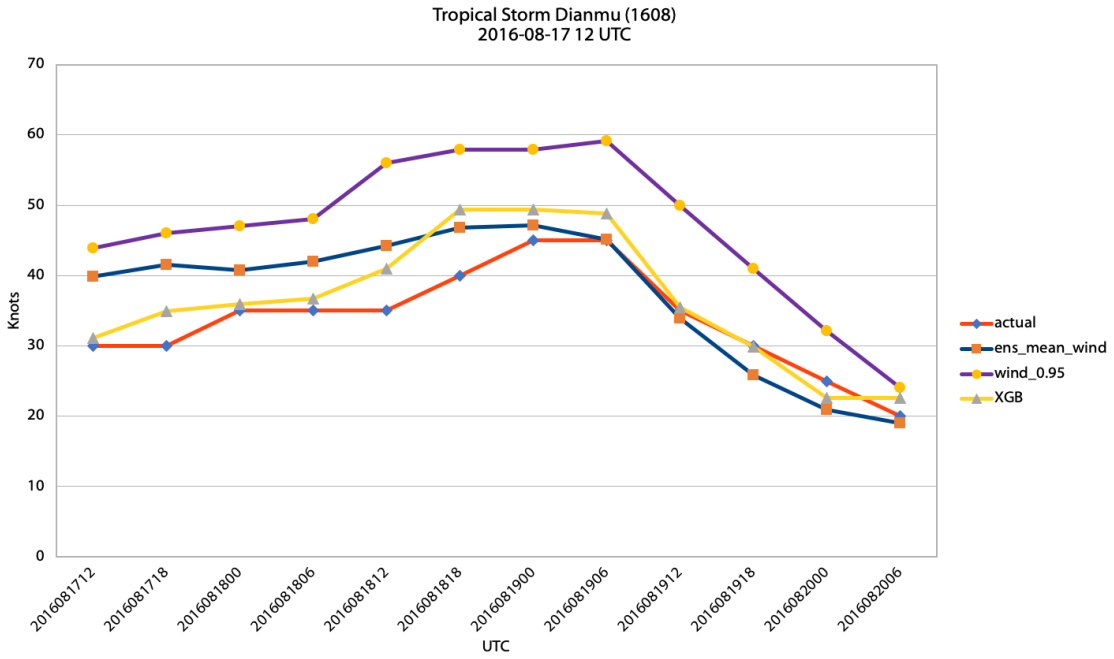

(a) Tropical Storm Dianmu (1608); Base Time 2016-08-17 12 UTC

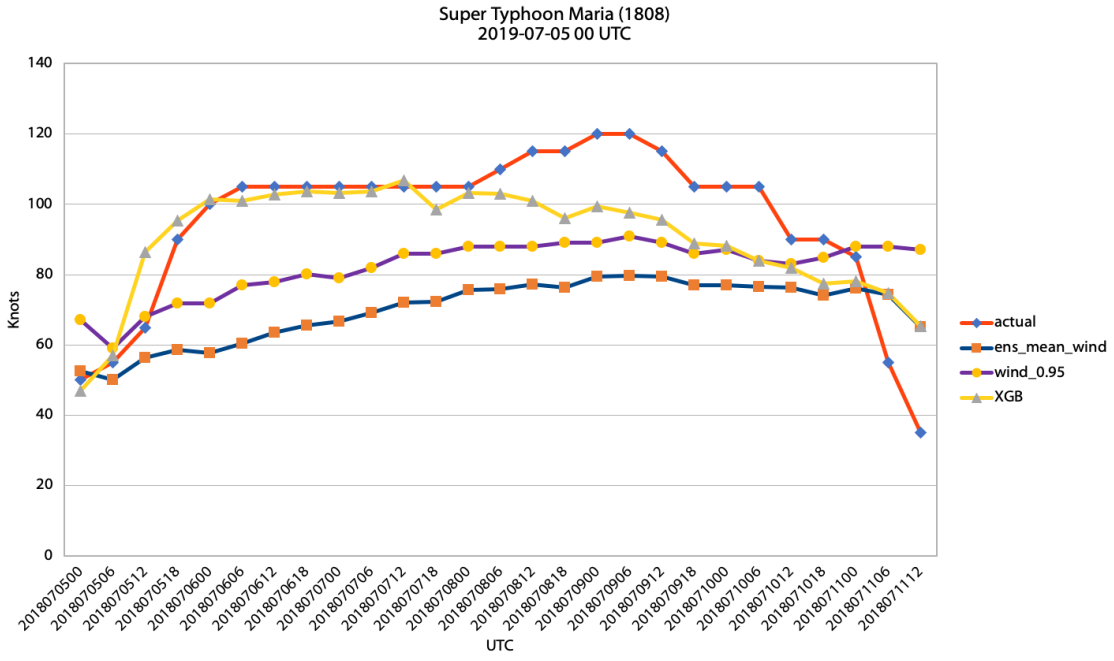

(b) Super Typhoon Maria (1808); Base Time 2018-07-05 00 UTC

Figure 13: Consensus XGBoost Model, ECMWF EPS Mean and 95th Percentile Forecast against HKO BT Intensity (Actual)

6 Discussion

Most TCs at typhoon strength or above were underestimated by ECMWF EPS as shown in Figure 1. This is also reflected in the preference of predictors in the XGBoost model (XGB), which considers stronger EPS percentiles as more important features. Systematic negative biases exist in ECMWF EPS even for the 75th percentile member. As the storm strength increases, the underestimation becomes more prominent. As explained by Marks (2015), strong typhoons attain a higher Ro so that cyclostrophic balance may represent the core structure better than the gradient wind balance. The maximum wind usually occurs at a small area around the eyewall. As suggested by Andersson and Hollingsworth (1988), these intense small-scale features may not be acknowledged by NWP models and may be rejected, resulting in a poor representation in severe storm structures.

The forecast performance analysis in Figure 10 shows that the Consensus XGB outperforms ECMWF EPS in all lead time hours. Among the EPS members, higher percentile members generally produce better forecasts than lower percentile members. The forecast error increases with the lead time as the predictability decreases due to initial errors. It is interesting to note that the forecast error saturates at T+84h for all but the 95th percentile member, which was surpassed by lower percentile members. We do not presume a reason behind this saturation, and we do not discuss it in detail in this paper as we aim at analyzing the performance of XGB. Nevertheless, XGB's dependence on lead time could possibly relate to this saturation, that XGB's forecast might be less influenced by the 95th percentile EPS member at longer lead time ranges. As the model training adopts the squared error loss function, it is justifiable that WIND_0.95 ranks top in the XGB feature importance as its forecast RMSE is the lowest among other percentiles adopted as predictors in the first 96 hours of forecast, followed by lower percentile members.

In Figure 8 we can observe that significantly different values of *max_depth* and *n_estimators* are preferred by weak and strong storms respectively. As we train up the XGB model with increasing values of *n_estimators*, the XGB model tends to produce a forecast with higher maximum wind regardless of the values of predictors. This could possibly be explained by the design of XGBoost in which later trees are produced to correct the errors of previous trees. As violent TCs are extreme cases and they constitute a small fraction among all TC

cases, the initial weak learners tend to align to the majority, i.e. the less violent storms. As more trees are added to the model, the later trees absorb the residual from previous trees and attempt to produce a better forecast. Due to the adoption of the squared error loss function, the errors of extreme cases amplify, shifting the forecast to higher wind speed ranges.

With the introduction of the Consensus XGB model, we are able to generate more accurate forecasts for weaker TCs without sacrificing the model's ability to alert major TCs and RI events. Yet, the Consensus model might have the shortcoming that an abrupt soar or plunge could be exhibited near the boundary of 63.8 knots when the TC undergoes gradual intensification from STS to T or weakening from T to STS. We suggest a blending technique, where two or more models are trained simultaneously with different parameters as in our Consensus model, while the weighting of individual models in the final forecast V is a non-binary function of some parameters (e.g. WIND_0.95):

$$V = \sum_{i}^{n} x_i v_i \tag{13}$$

In the current Consensus model, v_i is the forecast wind speed of the "Low" or "High" model while x_i is a binary function depending on the value of WIND_0.95. If a non-binary function for x_i with proper normalization is adopted, it is anticipated that the intensity forecast for all intensity ranges could be optimized.

An important message conveyed by the XGBoost feature importance function is the significance of latitude and longitude on the storm intensity. We will study three super typhoon cases forecast by the XGB model below.

The first case is Super Typhoon Maria (1808). As demonstrated in Figure 13b in Section 5, Maria underwent RI from July 5 - 6, 2018. The XGB model forecast, based on the 00 UTC run on July 5, 2018 of ECMWF EPS, successfully captured the RI event, though being 6 hours ahead of its occurrence. Meanwhile, the 95$^{\text{th}}$ percentile EPS member only forecast a gradual intensification. This behaviour of the XGB model could not be explained by the intensity predictors.

Another case is Super Typhoon Yutu (1826). Yutu was one of the strongest typhoons in 2018 and underwent RI from October 22 - 24, 2018, reaching a peak intensity of 135

knots. As shown in Figure 14a, XGB model forecast a significant intensification of Yutu, yet subpar to the RI standard. It forecast a peak intensity close to the actual peak, although delayed for 42 hours. The 95th percentile EPS member forecast a more moderate intensification, reaching only the upper boundary of a severe typhoon.

Super Typhoon Meranti (1614) was the strongest typhoon in 2016. As shown in Figure 14b, Meranti experienced prolonged RI from September 10 - 12, 2016. During the formation stage of the storm, XGB forecast a peak intensity of about 95 knots while the actual peak intensity was 135 knots. For the corresponding time period, the 95th percentile EPS member forecast merely about 70 knots, yielding a substantial absolute error of 65 knots. At the later stage of the run, the 95th percentile EPS member predicted Meranti to sustain its intensity as a typhoon. In reality, Meranti made landfall over Fujian on September 14 and rapidly weakened and dissipated on September 15. XGB was able to capture the weakening trend though it forecast a slower weakening process.

The above cases indicate that the EPS members influence could not fully explain the behaviour of the XGB model and the role of latitude and longitude was investigated.

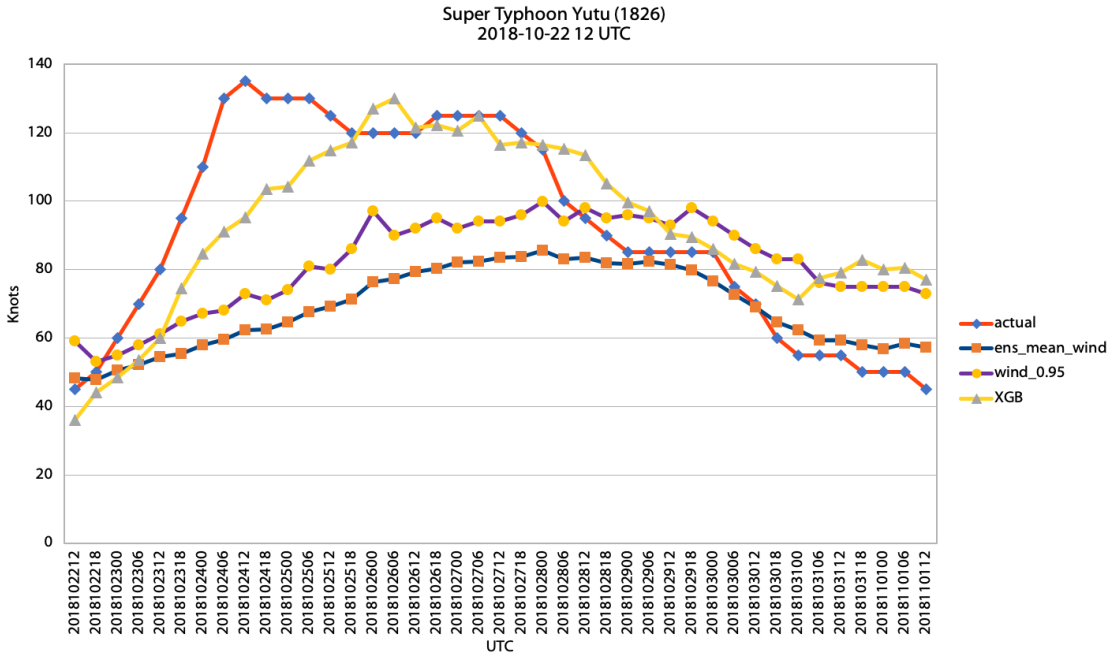

(a) Super Typhoon Yutu (1826); Base Time 2018-10-22 12 UTC

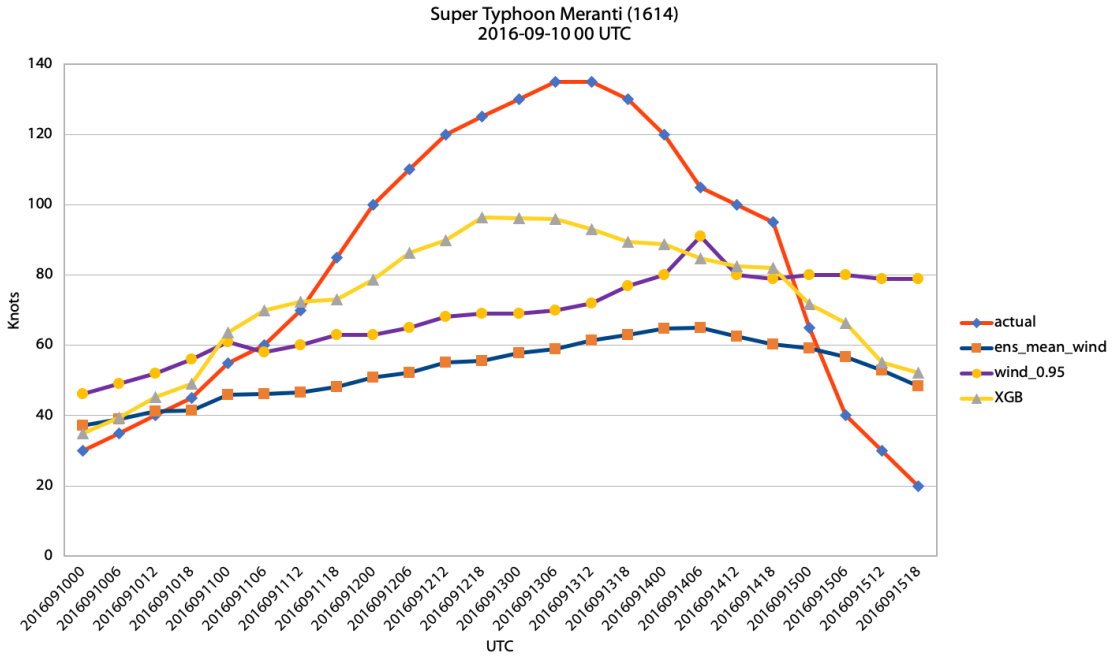

(b) Super Typhoon Meranti (1614); Base Time 2016-09-10 00 UTC

Figure 14: Consensus XGBoost Model, ECMWF EPS Mean and 95th Percentile Forecast against HKO BT Intensity (Actual)

Figure 15a shows the distribution of training cases reaching 100 knots or above. It should be noted that the coordinates reflect the ensemble mean latitude and longitude and are not necessarily equal to the BT coordinates. Furthermore, the same TC may be counted multiple times due to multiple EPS runs. This is to reflect that the XGB model includes the forecast data from all runs in the formulation of regression trees. Figure 15b shows the Gaussian Kernel-Density Estimate (KDE) based on the distribution in Figure 15a. It is observed that high densities of data points in the reddish regions in Figure 15b, which correspond to the seas east of the Philippines. This finding resembles the findings in identifying favourable regions for RI by Mei and Jiang. Although the two regions encompass different quantities, they are likely to be correlated as RI events may hint a high peak intensity. The reason for this favourable region's existence is not known and it is worth further investigation.

This region, however, could probably explain the behaviour of the XGB model in the above super typhoon cases. Figure 15b is overlaid with the ensemble mean forecast tracks of Maria, Yutu and Meranti in corresponding EPS runs in Figures 13b, 14a and 14b. The three typhoons were forecast to move in a generally northwesterly track as they passed through the reddish region in the forecast period.

As Maria was forecast to move into the reddish region, XGB predicted an abrupt intensification of 55 knots in 24 hours while WIND_0.95 was falling far behind the trend. XGB then forecast a slow weakening trend of Maria as it was forecast to gain in latitude and depart from the reddish region. The difference between the forecasts of XGB and WIND_0.95 narrowed as Maria transited to the bluish region where the high intensity data was less dense.

Meranti was in the reddish region in the initial stage of the EPS run as shown in Figure 15b. XGB forecast a significant intensification as it moved across the region. As Meranti was forecast to leave the region, XGB forecast a general weakening trend, whereas WIND_0.95 forecast a continuous slow intensification, hence narrowing the gap in forecast intensity.

For Super Typhoon Yutu, XGB captured the intensification trend better than WIND_0.95. XGB forecast Yutu's intensity to exceed 100 knots as it was forecast to move into the

reddish region. The XGB forecast intensity continued to climb and maintain a violent intensity until Yutu's ensemble mean track recurved and entered the bluish region where the XGB forecast intensity started to drop. While the EPS forecast Yutu to continue to weaken at the final period of the forecast, it is interesting to note that there was a final intensification in the XGB forecast, which coincided with the time of re-entrance into the reddish region when it took on the abnormal southwesterly track at the end of the forecast period.

Hence, we would conclude that the ensemble mean latitude and longitude influence the XGB forecast intensity likely in a way that corrects the forecast value based on EPS wind predictors through assessing the past intensity distribution in the vicinity of the forecast track.

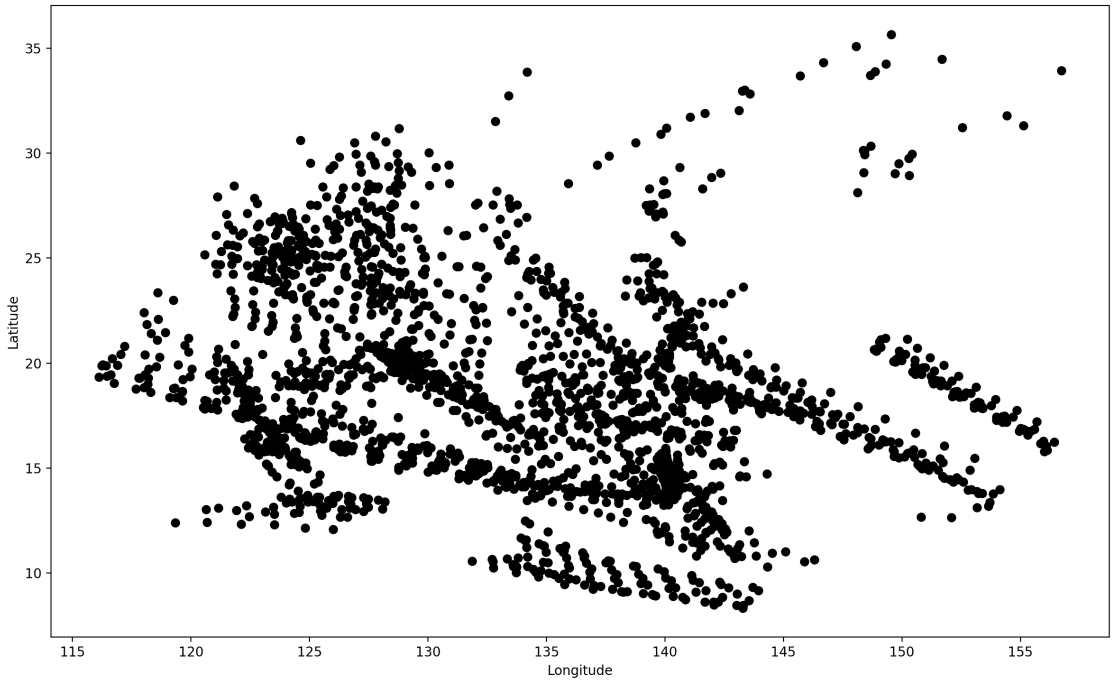

(a) Scatter Plot of Cases with BT Intensity Reaching 100 knots or above in Training Set

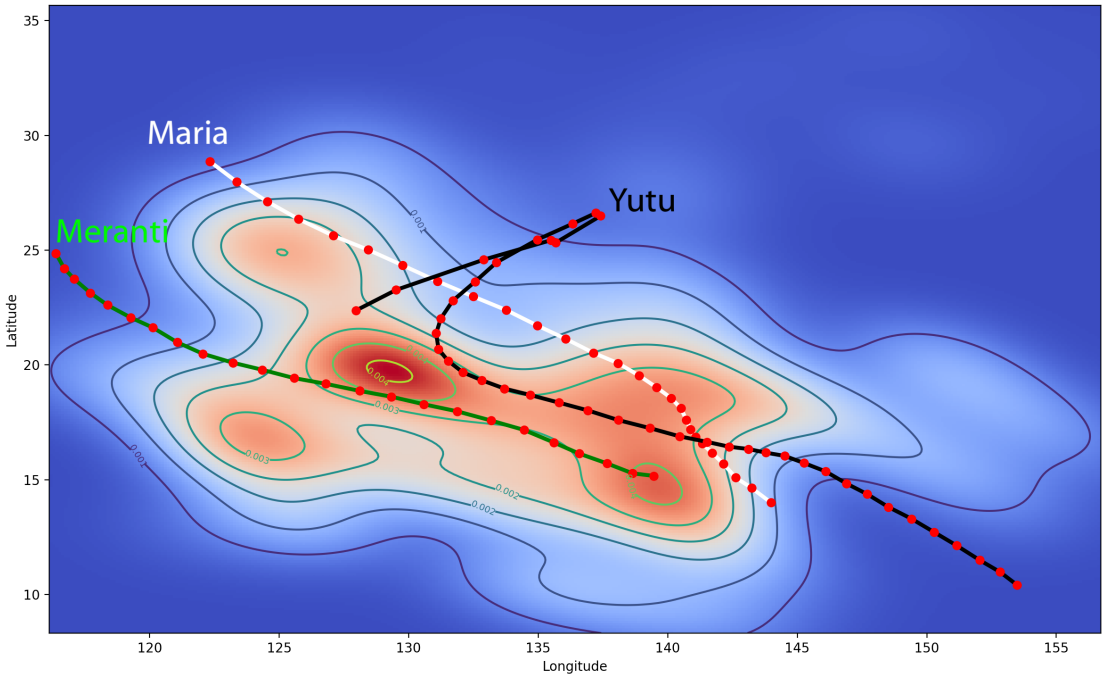

(b) Gaussian Kernel-density Estimate of 15a; Ensemble Mean Track of Super T Maria, Yutu and Meranti at Respective Base Time Shown in Figures 13b, 14a and 14b

Figure 15

However, this result also implies that the forecast accuracy of the XGB model is highly dependent on the ECMWF EPS forecast. The XGB model is unlikely to produce a good forecast if the input predictors are erroneous.

The EPS forecast for Meranti was mediocre as it did not predict Meranti to intensify into a super typhoon. The time of peak intensity was also erroneous, lagging behind the actual peak by 24 hours. XGB was better than EPS in the run in forecasting the trend of intensity change but the absolute error at its actual peak was still as large as 40 knots.

In the case of Maria, the XGB forecast for the first 72 hours was close to the actual intensity trend, yet it captured neither the second intensity peak nor the final RW stage. The EPS ensemble mean track was more northerly than the actual track. The mean track forecast Maria to make landfall south of Shanghai at night on July 11 and to skirt the coast of eastern China, before recurving to the Yellow Sea towards Korea. However, Maria finally made landfall over Fujian in the morning on July 11 and tracked deep inland and dissipated. The slow weakening trend forecast by XGB as depicted in Figure 13b was likely to be based on the recurving track, hence it was unable to capture the correct trend at the later forecast period.

A final case to mention is Yutu. The ensemble mean track on October 22, 2018 12 UTC is shown in Figure 17a. There was a recurvature followed by an uncommon twist to the southwest. The actual track of Yutu, however, was a westerly track across Luzon that turned northwards and finally dissipated in the South China Sea (SCS). It should be noted that the ensemble mean track was in fact inconclusive of any scenario forecast by the EPS members. As depicted in Figure 17b, the EPS members diverged into two clusters, with one forecasting a recurvature track and the other forecasting a westerly track. The ensemble mean track twisted to the southwest at the final stage as some EPS recurvature members died out, shifting the ensemble mean towards the westerly cluster. Such track is obviously a poor representation of the storm development, yet the XGB model apparently considered the track in its prediction and forecast an incorrect strengthening trend on October 31.

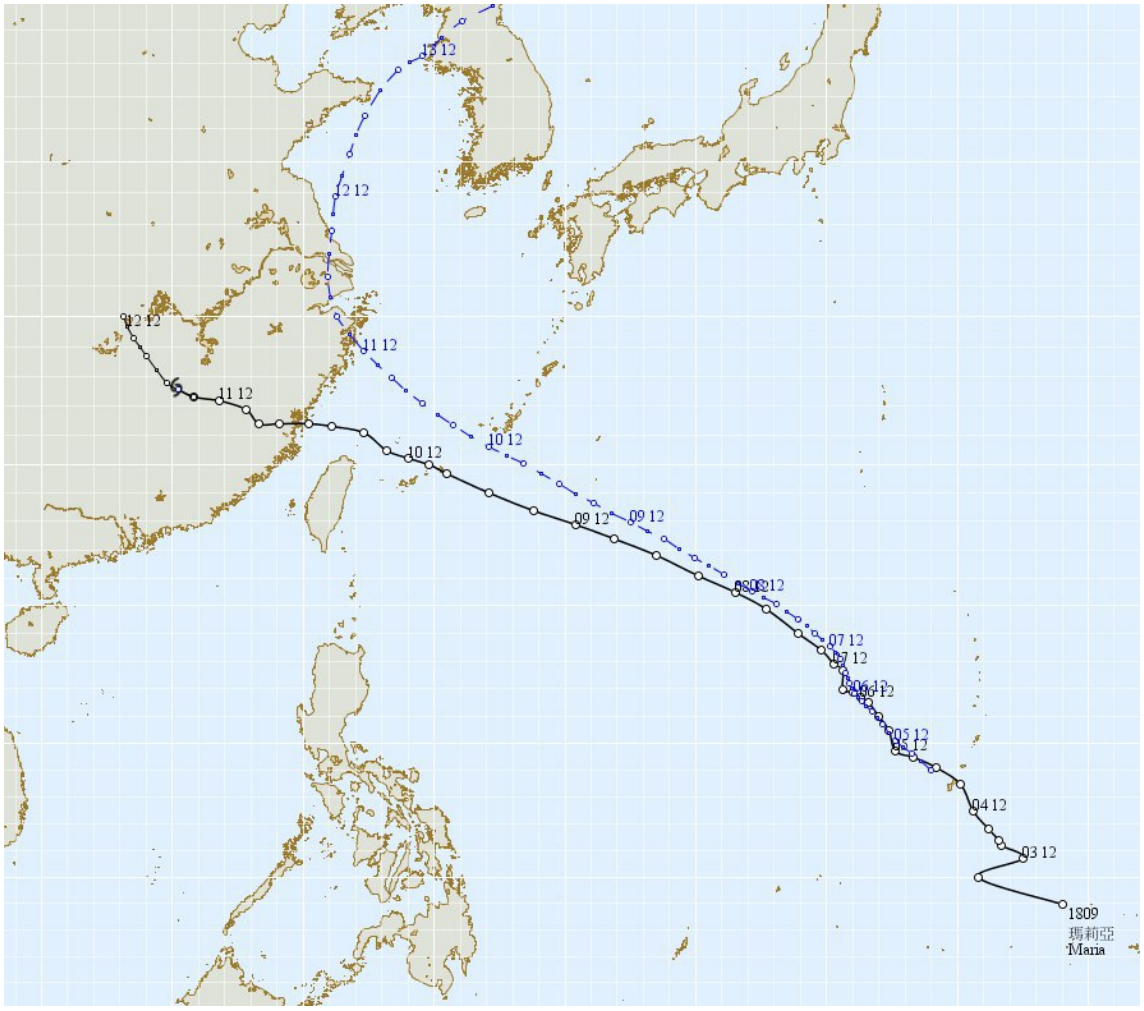

Figure 16: ECMWF EPS Ensemble Mean Track (Blue) and HKO Best Track (Black) of Super Typhoon Maria (1808); Base Time 2018-07-05 00 UTC (Credit: Hong Kong Observatory)

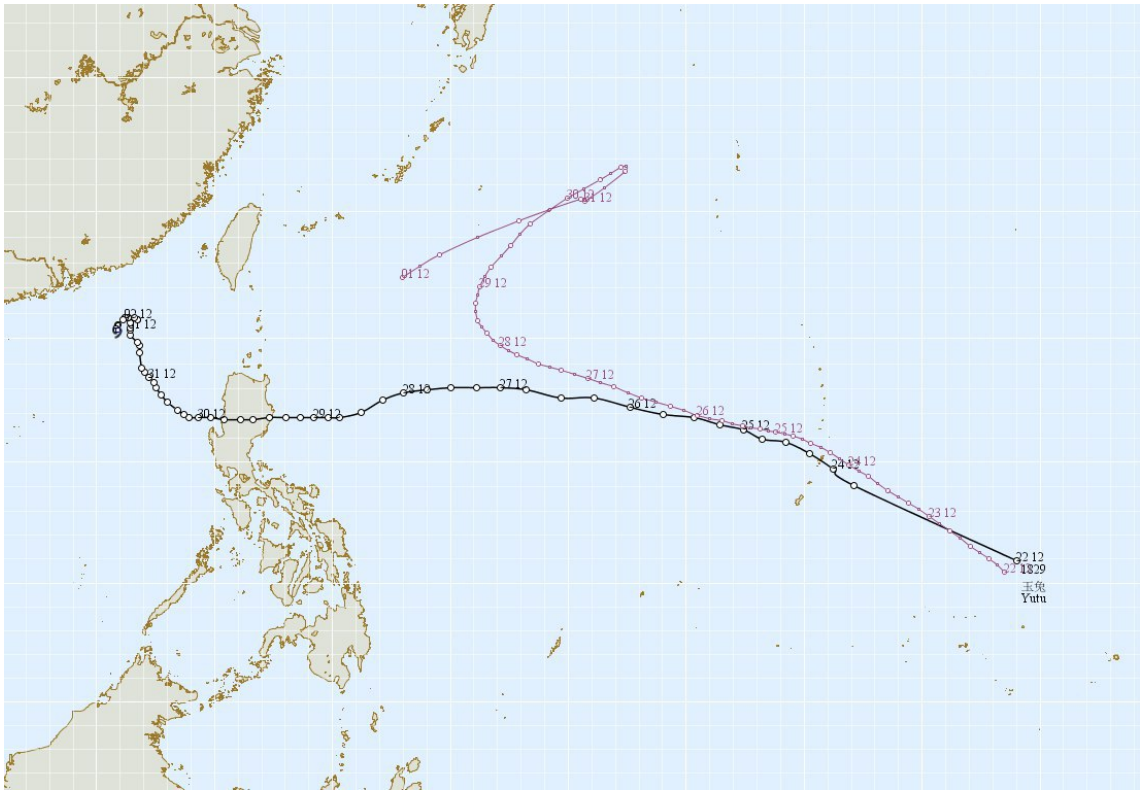

(a) ECMWF EPS Ensemble Mean Track (Blue) and HKO Best Track (Black) of Super Typhoon Yutu (1826); Base Time 2018-10-22 12 UTC (Credit: Hong Kong Observatory)

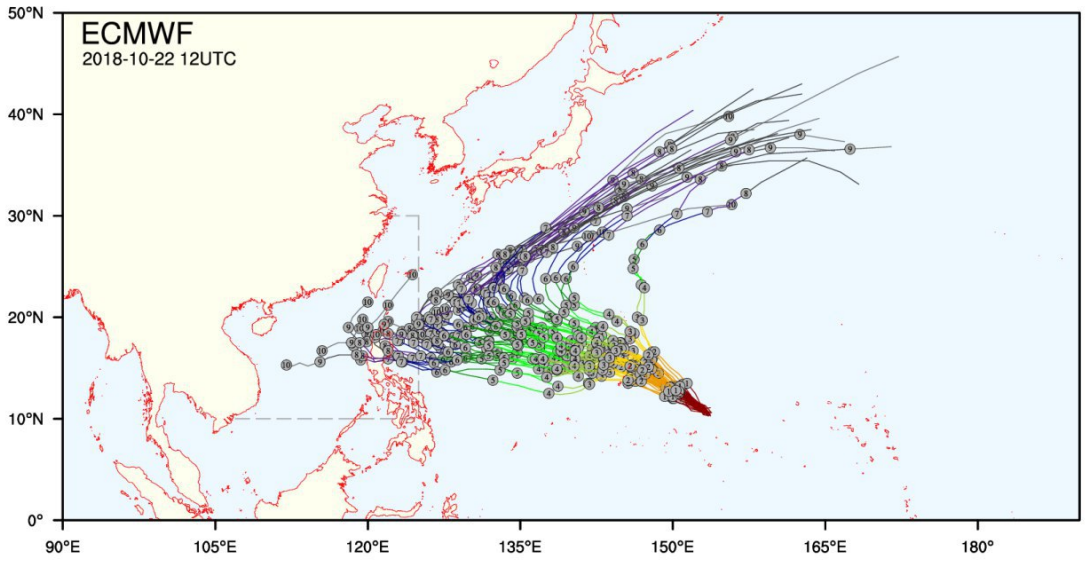

(b) ECMWF EPS Ensemble Member Tracks of of Super Typhoon Yutu (1826); Base Time 2018-10-22 12 UTC (Credit: Hong Kong Observatory)

Figure 17

Another limitation of the XGB model is that it might not be able to detect extreme cases. As the XGB forecast is based on past forecast and actual data, the forecast output is likely to be limited within the range of the past actual data. If an extremely violent typhoon formed where the forecast data was out of the past data range, XGB might not be able to extrapolate to forecast an extreme intensity.

The behaviour of the XGB model under extreme cases is not yet known. Looking ahead, we anticipate that by including more forecast data as TCs continue to form, the behaviour of the XGB model could be better understood. We also expect that the forecast performance of XGB will improve as more data is included as training cases. We also suggest a greater ensemble of predictors such as other NWP ensemble or deterministic models to be included in the machine learning model. While more features are being added to the model, one should note that there are scheduled updates in NWP models and their behaviours might change. XGBoost's sensitivity to each feature may also consequently change and the list of predictors and the feature importance should be updated on a timely basis to adapt to the changes in the predictors' behaviours.

7 Conclusion

In this paper, we presented a decision-tree-based machine learning method, namely XGBoost, to forecast the maximum wind of tropical cyclones based on ECMWF EPS forecast data. The forecast data includes TCs in the western North Pacific in January 1, 2015 to August 3, 2019. We found out that ECWMF EPS systematically underestimated the intensity of tropical cyclones, especially stronger TCs. The XGBoost model identified stronger percentiles ECWMF EPS members as important features for its forecast. It was also found that the forecast hour and location of the TC may influence the forecast of the XGBoost model.

We developed a Consensus XGBoost model which is based on two different XGBoost models with different training parameters due to their differential behaviours in forecasting TCs with different intensities. We showed that the Consensus model was in general performing better than individual models. It also attained a smaller forecast error than

ECMWF EPS. The XGBoost model has also the potential to capture RI cases.

We presented three super typhoon cases, namely Maria, Yutu and Meranti to discuss the behaviours of the XGBoost model. Except the ECMWF EPS wind members being major contributors, we discovered some regions over the Pacific might be beneficial to the development of strong TCs and was consistent with the findings of previous research. We believe that XGBoost might have the potential to identify regions which favour strong TC development and would accordingly adjust its forecast.

Finally, we discussed the limitations of the XGBoost model, mainly due to the high dependency on ECMWF EPS forecast. We recommend a further optimization on the model parameters and suggest including other NWP models to be predictors in the hope of further improvement in the model's forecast performance.

The results of this research showed that machine learning models have the potential to improve intensity forecast in tropical cyclones. A feature of this method is that it combines real-time forecast with analogical methods. It could learn to forecast better by considering past experience with similar forecast conditions. We hope this method will pave a new avenue in tropical cyclone forecast techniques and we look forward to sparking more research in pursuit of greater forecast accuracy.

Acknowledgements

This project was completed under the one-year placement programme offered by the Hong Kong Observatory. I wish to thank the Department of Physics of The Chinese University of Hong Kong and the Hong Kong Observatory, for offering me the internship in the Observatory and allowing me to apply what I learnt in lessons to practical uses. I am very grateful for having the opportunity to intern at the Observatory for a year, which reaffirmed my interest in meteorology.

I would like to thank Professor Francis Tam, the advisor of my project. He has provided guidelines and suggestions for me to improve my project. I am also very grateful for his full support and encouragement on my work. Without his support, it would not be able for me to explore in the world of meteorology and to discover and learn knowledge that is out of textbooks.

I would like to express my sincere gratitude to Mr. Wong Wai-kin, my mentor and advisor in the Hong Kong Observatory. I would like to especially thank Mr. Wong for his insightful and invaluable advice and suggestions on my project. He beaconed and inspired me throughout my year of internship in the Hong Kong Observatory. Without his patient and assiduous guidance, this project would not be possible.

I would like to acknowledge Ms. Jessica Acuña, my Language and Communication advisor. She was really helpful in offering advice and comments on the language of this project report. She let me learn more about academic writing and pick up skills in writing a better research paper.

I would like to offer my great appreciation to Mr. Au-yeung Kin-chung, Mr. Nick Shek and Mr. Cho Shing-kei for their assistance and technical support on this project. They helped to handle numerous data and construct the machine learning model. They also provided inspiring and useful comments on the optimization of the model.

I wish to extend my thanks to Mr. Woo Wang-chun, Mr. Chong Man-lok, Mr. Lam Ming-chun, Mr. Chan Ngo-hin, staff and intern companions in the Hong Kong Observatory for your hospitality and kindness that you made my year in the Observatory.

List of Acronyms

BT Best Track

ECMWF European Centre for Medium-Range Weather Forecasts

EPS Ensemble Prediction System

HKO Hong Kong Observatory

KDE Kernel-density Estimate

JMA Japan Meteorological Agency

MAE Mean Absolute Error

NWP Numerical Weather Prediction

RI Rapid Intensification

RMSE Root-mean-square Error

RW Rapid Weakening

SCS South China Sea

SST Sea Surface Temperature

ST Severe Typhoon

STS Severe Tropical Storm

Super T Super Typhoon

T Typhoon

TC Tropical Cyclone

TD Tropical Depression

TS Tropical Storm

UTC Coordinated Universal Time

VWS Vertical Wind Shear

XGB XGBoost (Extreme Gradient Boosting)

References

Andersson, E., & Hollingsworth, A. (1988). Typhoon bogus observations in the ECMWF data assimilation system. (148), 25. doi:10.21957/2wlaltiso

Bonavita, M., Dahoui, M., Lopez, P., Prates, F., Hólm, E., Chiara, G. D., … Ingleby, B. (2017). On the initialization of tropical cyclones. (810). doi:10.21957/insgrw8u6

Buizza, R. (2002). *Chaos and weather prediction*. ECMWF. Retrieved from https://www.ecmwf.int/node/16927

Chen, P. Y., & Chan, S. T. (2010). Use of the JMA Ensemble Prediction System for Tropical Cyclone Intensity Forecasting. In *ESCAP/WMO typhoon committee annual review 2008* (pp. 276–285).

Chen, T., & Guestrin, C. (2016). XGBoost: A scalable tree boosting system. *CoRR*, *abs/1603.02754*. arXiv: 1603.02754. Retrieved from http://arxiv.org/abs/1603.02754

Doocy, S., Dick, A., Daniels, A., & Kirsch, T. D. (2013). The human impact of tropical cyclones: A historical review of events 1980-2009 and systematic literature review. *PLoS Currents*, *5*. doi:10.1371/currents.dis.2664354a5571512063ed29d25ffbce74

Giffard-Roisin, S., Yang, M., Charpiat, G., Bonfanti, C., Kégl, B., & Monteleoni, C. (2020). Tropical cyclone track forecasting using fused deep learning from aligned reanalysis data. *Frontiers in Big Data*, *3*, 1. doi:10.3389/fdata.2020.00001

Holliday, C. R., & Thompson, A. H. (1979). Climatological characteristics of rapidly intensifying typhoons. *Monthly Weather Review*, *107*(8), 1022–1034. doi:10.1175/1520-0493(1979)107<1022:CCORIT>2.0.CO;2. eprint: https://doi.org/10.1175/1520-0493(1979)107<1022:CCORIT>2.0.CO;2

Hu, C. M., Duan, Y. H., Yu, H., Yu, R. L., & Du, B. Y. (2005). Huanan diqu redaiqixuan denglu qian qiangdu tubian de dachidu huanjing zhenduan fenxi [The diagnostic

analysis of the rapid change in tropical cyclones intensity before landfall in south China]. *Redai qixiang xuebao*, *21*(4), 377–382.

Kaplan, J., & DeMaria, M. (2003). Large-scale characteristics of rapidly intensifying tropical cyclones in the north atlantic basin. *Weather and Forecasting*, *18*(6), 1093–1108. doi:10.1175/1520-0434(2003)018<1093:LCORIT>2.0.CO;2. eprint: https://doi.org/10.1175/1520-0434(2003)018<1093:LCORIT>2.0.CO;2

Kaplan, J., Rozoff, C. M., DeMaria, M., Sampson, C. R., Kossin, J. P., Velden, C. S., … Solbrig, J. E. (2015). Evaluating environmental impacts on tropical cyclone rapid intensification predictability utilizing statistical models. *Weather and Forecasting*, *30*(5), 1374–1396. doi:10.1175/WAF-D-15-0032.1. eprint: https://doi.org/10.1175/WAF-D-15-0032.1

Loridan, T., Crompton, R., & Dubossarsky, E. (2017). A machine learning approach to modeling tropical cyclone wind field uncertainty. *Monthly Weather Review*, *145*(8), 3203–3221. Copyright the Author(s) 2017. Version archived for private and non-commercial use with the permission of the author/s and according to publisher conditions. For further rights please contact the publisher. doi:10.1175/MWR-D-16-0429.1

Lynch, P. (2008). The origins of computer weather prediction and climate modeling. *Journal of Computational Physics*, *227*(7), 3431–3444. Predicting weather, climate and extreme events. doi:https://doi.org/10.1016/j.jcp.2007.02.034

Marks, F. (2015). Tropical cyclones and hurricanes | hurricanes: Observation. In G. R. North, J. Pyle, & F. Zhang (Eds.), *Encyclopedia of atmospheric sciences (second edition)* (Second Edition, pp. 35–56). doi:https://doi.org/10.1016/B978-0-12-382225-3.00163-8

Mei, S. L., & Jiang, J. (2012). Xibei taipingyang redaiqixuan xunsu zengqiang tezheng ji qi yingxiang yinzi [Characteristics and influence factors of rapid intensification of tropical cyclones in the western North Pacific]. *Redai qixiang xuebao*, *28*(1), 1–11.

Natekin, A., & Knoll, A. (2013). Gradient boosting machines, a tutorial. *Frontiers in neurorobotics*, *7*, 21. doi:10.3389/fnbot.2013.00021

Richman, M. B., Leslie, L. M., Ramsay, H. A., & Klotzbach, P. J. (2017). Reducing tropical cyclone prediction errors using machine learning approaches. *Procedia Computer Science*, *114*, 314–323. Complex Adaptive Systems Conference with Theme: Engineering Cyber Physical Systems, CAS October 30 – November 1, 2017, Chicago, Illinois, USA. doi:https://doi.org/10.1016/j.procs.2017.09.048

Shaiba, H., & Hahsler, M. (2016). Applying machine learning methods for predicting tropical cyclone rapid intensification events. *Research Journal of Applied Sciences, Engineering and Technology*, *13*(8), 638–651.

Ventham, J. D., & Wang, B. (2007). Large-scale flow patterns and their influence on the intensification rates of western north pacific tropical storms. *Monthly Weather Review*, *135*(3), 1110–1127. doi:10.1175/MWR3327.1. eprint: https://doi.org/10.1175/MWR3327.1

Wang, B., & Zhou, X. (2008). Climate variation and prediction of rapid intensification in tropical cyclones in the western North Pacific. *Meteorology and Atmospheric Physics*, *99*(1-2), 1–16. Copyright - Springer-Verlag 2008; Last updated - 2014-08-09; SubjectsTermNotLitGenreText - Pacific Ocean. Retrieved from http://easyaccess.lib.cuhk.edu.hk/login?url=https://search-proquest-com.easyaccess2.lib.cuhk.edu.hk/docview/220841980?accountid=10371

Wang, D., Liang, X., Ying, Z., & Wang, B. (2008). A comparison of two tropical cyclone bogussing schemes. *Weather and Forecasting - WEATHER FORECAST*, *23*. doi:10.1175/2007WAF2006094.1

Zamani Joharestani, M., Cao, C., Ni, X., Bashir, B., & Talebiesfandarani, S. (2019). PM2.5 prediction based on random forest, XGBoost, and deep learning using multisource remote sensing data. *Atmosphere*, *10*(7), 373. doi:10.3390/atmos10070373